ELECTRIC FIELD-INDUCED ISOMERIZATION OF AZOBENZENE CONTAINING MIXED SELF-ASSEMBLED MONOLAYERS BY ATOMIC FORCE MICROSCOPY

by

Anish Dhungana, M.S.

A thesis submitted to the Graduate Council of
Texas State University in partial fulfillment
of the requirements for the degree of
Master of Science
with a Major in Physics
August 2021

Committee Members:

Yoichi Miyahara, Chair

Wilhelmus J Geerts

William J. Brittain

FAIR USE AND AUTHOR'S PERMISSION STATEMENT

Fair Use

Duplication Permission

ACKNOWLEDGEMENTS

The completion of this thesis would not have been possible without the help from the following people I want to give my thanks to:

My research advisor Dr. Yoichi Miyahara, for his constant support and guidance during the last two years. During my degree program, he has mentored me on a daily basis, from which I have learned a lot and have been able to shape myself to become a better scholar. His advice and encouragement will be crucial in my future career development.

I would also like to thank my committee members Dr. Wilhelmus J Geerts and Dr. William J. Brittain, for putting their time and effort into offering insights into my work. I would like to thank Dr. Casey Smith, the entire Nanofabrication Research Service Center, and the entire Analysis Research Service Center (ARSC) staff at Texas State University for providing training on the various characterization equipment. I would like to thank Mitchell Ford for characterizing my sample with the modified JEOL AFM. I would like to thank Rigo Mayorga-Luna, who helped to take the optical images and SEM of the samples and to prepare the samples. Lastly, I would like to thank my group members: Dr. Dip N Mahato, Binod D.C., Noah, Nischal, Gabe R. Mestas, Johnathan, and John.

TABLE OF CONTENTS

Page

LIST OF TABLES

Table **Page**

LIST OF FIGURES

Figure **Page**

LIST OF ABBREVIATIONS

Abbreviation	Description
AB	Azobenzene
UV	Ultraviolet
SAMs	Self-Assembled Monolayers
TBA	3,3′,5,5′-tetra-tert-butylazobenzene
TSG	Template Stripped Gold
Az11	E-11-(4(-phenyldiazenyl) phenoxy) undecane-1-thiol
C10	1-Decanethiol
mSAMs	mixed Self-Assembled Monolayers
FTIR	Fourier Transform Infrared Spectroscopy
AFM	Atomic Force Microscopy
KPFM	Kelvin Probe Force Microscopy
N	Nitrogen
C	Carbon
eV	electron Volt
STM	Scanning Tunneling Microscopy
Au	Gold
ARSC	Analysis Research Service Center
SRO	Shared Research Operations

NRSC	Nanofabrication Research Service Center
RFM	Royal F. Mitte
As	Arsenic
Si	Silicon
SiO2	Silicon dioxide
Å	Angstrom
uL	microliter
mM	millimolar
mL	milliliter
g	gram
ATR	Attenuated Total Reflectance
DFM	Dynamic Force Microscopy
FM	Frequency Modulation
CPD	Contact Potential Difference
um	micrometer
nm	nanometer
PiFM	Photoinduced Force Microscopy

ABSTRACT

Azobenzene is the organic compound that undergoes a reversible transformation from the thermodynamically stable trans (E) to cis (Z) form via light, external electric field, and heat. Due to this property of Azobenzene can be used in motor sensors, optical storage applications, and motor actuators. The transformation due to light is called photoisomerization. While the photoisomerization of Azobenzene in the solution and gas phase has been well understood, Azobenzene anchored to a solid substrate is not as well understood due to complexity arising from their surrounding environment such as steric hindrance and excitonic coupling between azobenzene molecules. Self-Assembled Monolayers (SAMs) of Azobenzene is the technique to immobilize the azobenzene molecule by attaching the azobenzene containing molecule with thiol group(-SH), in which sulfur covalentely bonds with Au. This work investigates the photoisomerization of Azobenzene containing mixed self-assembled monolayers (mSAMs) on template stripped gold/Si/SiO2. We were able to successfully prepare azobenzene-containing mSAMs on template stripped gold, as validated by Fourier Transform Infrared Spectroscopy. Using Atomic Force topography measurements, photoisomerization of the azobenzene molecules is observed.

1. INTRODUCTION

The semiconductor industry is constantly miniaturizing to fit more and more transistors onto a single chip. Smaller device size is not only the desired aim from the user's perspective, but it also allows the electronics to function at lower voltages and currents [1], resulting in improved efficiency. When striving for nanometer-sized devices, however, this top-down method will hit its limits [2].

Therefore, so-called molecular switches and machines are an active field of research [3], [4]. Such molecules are nanometer-sized and modern chemistry can synthesize a huge variety of compounds for various possible applications.[3] Molecular switches are molecules that change their structure reversibly by external stimuli such as light, external electric field, or chemical energy [5]. Out of the various molecular switch studied, photoswitchable molecules are well-studied molecules.[6] Since its reversible isomerization was originally described some eight decades ago[7], azobenzene [8]–[13] (A.B.) (IUPAC name: diphenyldiazene) has undoubtedly been the most researched photoswitch due to its simple chemical structure and unusual properties. The stable trans state and the metastable cis state are the two conformations of the AB molecule [14]. The thermodynamically stable trans (E) isomer of AB isomerizes [15], [16] to the cis (Z) form when exposed to UV ($\lambda \approx 365$ nm) light (Figure1). When the UV source is removed, the metastable cis state returns to the trans state. Though thermal re-isomerization is slow, heating or exposure to visible ($\lambda \approx 430$ nm) light may considerably speed it—in fact, both trans–cis and cis–trans processes can be completed in picoseconds in solution phase [17]–[19]. In addition, The reversible isomerization of AZ molecules can be induced by applying an Electric Field using Scanning Tunneling Microscope [20].

As part of the initial attempts to functionalize surfaces with azobenzene, the molecule was evaporated directly onto a metal surface; however, the photoisomerization was severely quenched by the interaction with the substrate [21], [22]. Decoupling between the switch (AB moiety) and the surface is thus necessary. One approach was to use bulky endgroups to decouple the flat-lying azobenzene from the substrate. However, the photoisomerization efficiency was orders of magnitude lower than azobenzene in solution [23].

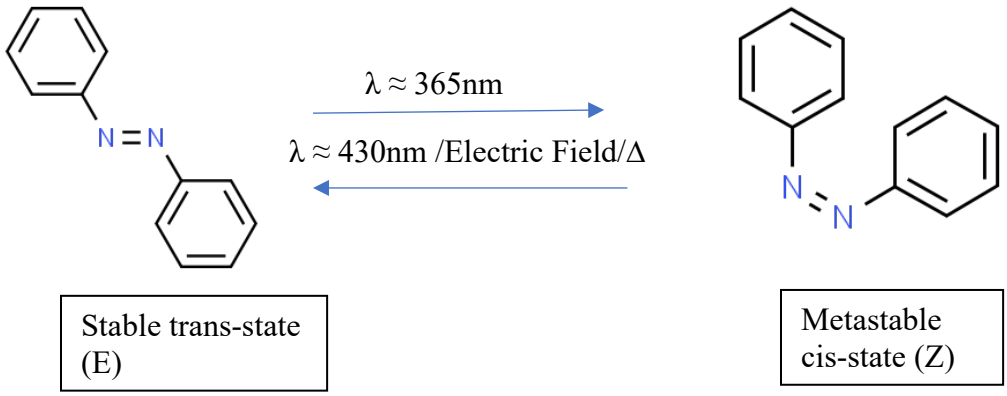

Figure 1: Reversible switching of E/Z by application of UV light, visible light, Electric Field, and Δ

One alternative way to achieve distance between the AB moiety and the substrate is molecular self-assembly. The ordered 2D arrangements of molecules on a solid surface are known as self-assembled monolayers (SAMs) [24], [25]. One example of AB-functionalized SAMs can be AB-terminated alkyl chains [26] with thiol(-SH) as a head group on the noble metal substrate (e.g., Gold).

The photoisomerization of azobenzene-alkanethiolate-SAMs is inhibited due to the steric hinderance[6], [27], [28] (Figure2.) and excitonic coupling between the chromopores when the AB moieties are densely packed [27]. Excitonic coupling is an interaction of excited states of chromophores resulting in excited state to delocalize over all

chromophores as an exciton when two or more identical chromophores are put near together [27] . By mixing two SAMs, one with AB containing alkyl chains as a switch, and other with alkyl chains as a spacer, we can solve this problem [6], [29]. Several groups have studied photoisomerization of this SAMs [30]–[32].

Compared with the photoswitching properties, electric field-induced switching has not been well studied. Wen, Jin et al. has investigated the electric field switching of

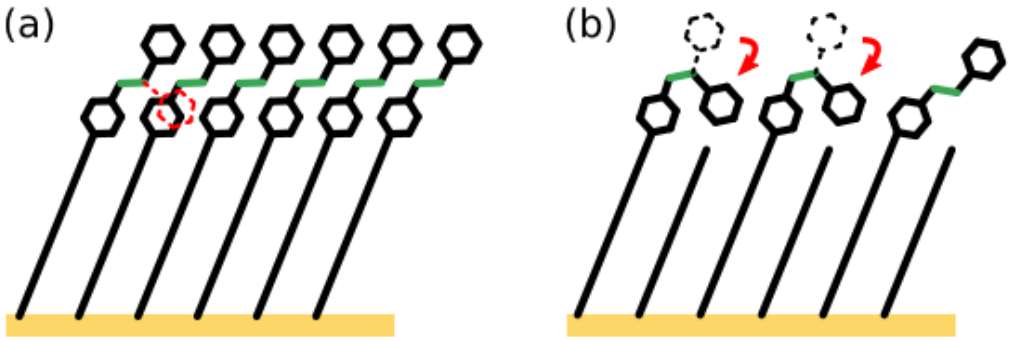

Figure 2: Schematic of SAMs of azobenzene-alkanethiols on gold. (a) Isomerization is inhibited in a densely-packed SAM because there is too little space between the chromophores. (b) Isomerization can occur in SAMs with reduced density of chromophores[14].

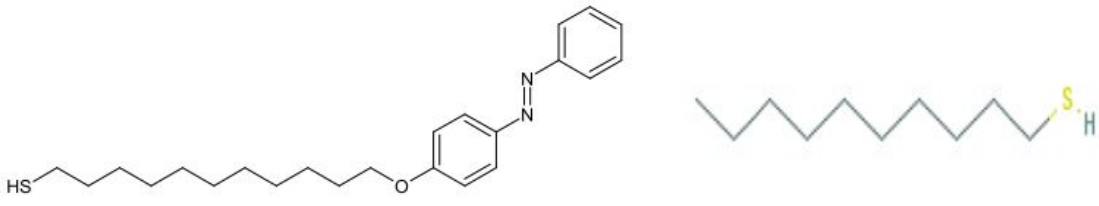

Figure 3: Chemical Structure of Az11(left) [14] and C10 (right) [33]

azobezene containing self-assembled monolayers by theoretical calculation[34]. Besides

this, there is one experimental work regarding the electric field switching of 3,3′,5,5′-tetra-tert-butylazobenzene(TBA) using Scanning tunneling microscope[20]. In addition, Azobenzene containing mSAMs on top of low-cost Template Stripped Gold on SiO2/Si (TSG) substrate have been rarely investigated [35]. In this work, I investigated the Electric Field-Induced Isomerization of mixed self-assembled monolayers (mSAMs) of E-11-(4(-phenyldiazenyl) phenoxy) undecane-1-thiol (Az11) (as shown in Fig 3)and 1-Decanethiol (C10) (Fig 3) on top of the template stripped gold(TSG) on SiO2/Si substrates by applying local electric field by atomic force microscopy tip and subsequent Kelvin Probe Force Microscopy. The focus is the effect of electric field strength, the surrounding environment of azobenzene moieties, and the substrate morphology. The characterization techniques for mixed Self-Assemble Monolayers of Azobenzene-thiol and decane-thiol are Fourier Transform Infrared Spectroscopy (FTIR), Atomic Force Microscopy (AFM), and Kelvin Probe Force Microscopy (KPFM). The chemical composition of the used compounds is confirmed using FTIR spectroscopy. The FTIR spectra of the neat(solid) Az11 used to make the mSAMs are compared to the spectra obtained from the mSAM on TSG substrates. AFM is used to analyze the surface of the mSAMs before and after irradiation in order to detect any differences in the film morphology during isomerization. A local electric field is applied to a certain area on the mSAM by the AFM tip. Then, the surface potential of this mSAMs is characterized by KPFM.

2. LITRATURE REVIEW

In this chapter, I will discuss the work that had been done previously. I will begin by discussing the work on the Self-Assembled Monolayers (SAMs) of Azobenzene derivatives. Moving on, I will discuss the photoisomerization of AB-bearing mixed SAMs. I will go into the reversible Electric-Field Induced Isomerization of AB-bearing mixed SAM later.

2.1 Photoisomerization mechanisms of Azobenzene

Azobenzene is a molecule that constitutes two phenyl rings which are linked by two nitrogen atoms [36] (see Figure1.). A nearly planar trans-state and non-planar 3D cis state in the electronic ground state are the two configurations [37], [38] of Azobenzene molecules. The trans- conformation has a 0.6 eV lower total energy than the cis-conformation, and a 1.6 eV barrier separates the two types (isomerization from trans- to cis-)[39]. In both the solution and gas phase, they undergo reversible photoinduced isomerization, which is well understood[15], [16], [18], [40]–[43]. 3.40 eV ($\lambda \approx 365$ nm) is required to convert from trans to cis isomer, whereas 2.95 eV ($\lambda \approx 420$ nm) is required in the other way [36].

It is generally understood that photoisomerization takes place on an excited state potential energy surface, which intersects with the ground state potential energy surface in a conical intersection [15], [16], [18], [40]–[43]. Theoretically, two distinct methods for photoisomerization have been postulated (see Figure 4.): the so-called rotation mechanism[41], which is a twisting around the N-N bond (change of angle ω), and the inversion method[40], which is an in-plane rotation of the C-N-N (α angle). The rotation

pathway has been linked to a $S_0 \longrightarrow S_2$ excitation ($\pi \longrightarrow \pi^*$), whereas the inversion pathway has been linked to a $S_0 \longrightarrow S_1$ excitation ($n \longrightarrow \pi^*$). The HOMO⟶LUMO excitation dominates the $S_0 \longrightarrow S_1$ transition, whereas the HOMO-1⟶LUMO excitation dominates the $S_0 \longrightarrow S_2$ transition [36].

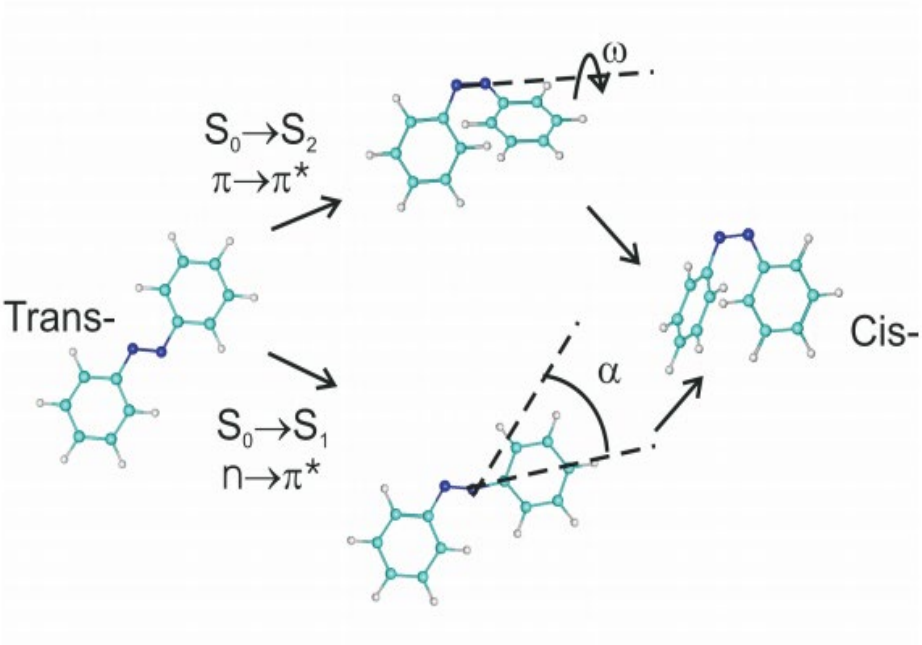

Figure 4: Schematics of photoisomerization: inversion and rotation paths are shown. Relevant conformation coordinates are the angle ω for the rotation mechanism (rotational axis is the N=N bond), and the angle α for the inversion (rotational axis perpendicular to the drawing plane) [36].

2.2 Self-Assembled Monolayers of Azobenzene

Azobenzene which is a well-studied molecules as the molecular switches exists in two conformations: the thermodynamically stable trans (E) state and metastable cis state (Z) [44]. Molecules that are isomerized upon external stimuli such as light, electric field, or pH value are called molecular switches [5], [20]. When light of various wavelengths

shines a molecule, it undergoes photoisomerization, which causes the conformation of the molecules to alter [14].

Anchoring the molecules which acts as a molecular switch onto solid surface has many applications. One of the simplest ways to accomplish this is by self-assembly of molecules.[14] Ordered arrays of molecules on a solid(substrate) surface are known as self-assembled monolayers (SAMs), which are nanometer-sized in units[24], [25]. SAMs have the following important properties: 1) it covers the whole surface of the substrate with a single monolayer. 2) it depends upon the binding of the molecules to the surface and intermolecular forces. 3) it consists of three parts (Figure 5.): Head group on the surface, a functional terminal group that forms the film's outer surface, and an alkyl chain that binds head to the terminal group. We used alkanethiols on Template Stripped Gold on Si/SiO2 substrate. There is a covalent bond between a thiol (-SH) group and gold, forming a gold thiolate bond [25], [45].

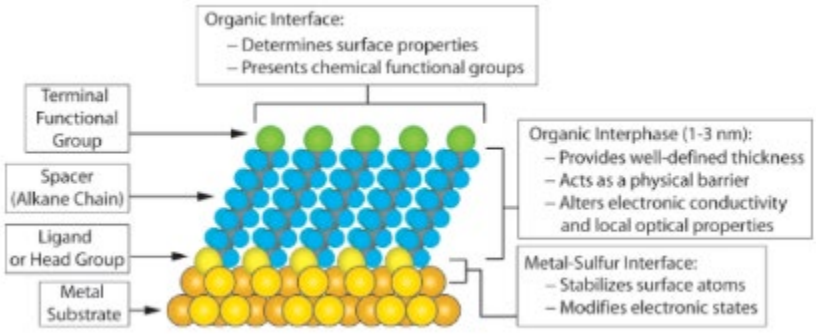

Figure 5: Schematic diagram of an ideal, single-crystalline SAM of alkane thiolates supported on a gold (111) surface. The Anatomy and the characteristics of the SAM are highlighted [45].

2.2.1 Mechanism of SAM Formation:

There are two steps in the formation of the SAMs: an adsorption of an anchoring chemical group to the surface, and a crystallization process. Then, there is a formation of strong gold thiolate bond (44 kcal/mol ≡ 1.9 eV) [46] as there is a bonding between sulfur head group and gold surface.

$$\mathrm{Au} + \mathrm{HS(CH_2)_nX} \xrightarrow{-\left(\frac{1}{2}\right)\mathrm{H_2}} \mathrm{Au - S(CH_2)_nX} \quad (1)$$

Due to the oxidation, the adsorption solutions often contain Disulfides which leads to same gold thiolate type as thiols:

$$\mathrm{Au} + \frac{1}{2}\mathrm{X(CH_2)_nSS(CH_2)_nX} \longrightarrow \mathrm{Au - S(CH_2)_n\,X} \quad (2)$$

The second process involves diffusion or exchange, which increases order in the molecular layer on a day-to-day basis. SAMs with domain sizes on the order of 100 nm^2 have been discovered using atomic force microscopy (AFM) and scanning tunneling microscopy (STM) [25].

2.3 Photoisomerization of Self-Assembled Monolayers

It is required to immobilize AB onto solid supports in order to fully utilize its potential, with the ultimate objective of manufacturing functioning photoresponsive materials [6]. The majority of research has focused on the preparation of SAMs[24], [47]–[49] of the molecules with AB ligands on noble metals and silicon because of the technical significance of these substrates and the successful monolayer forming techniques on their surfaces. Though sulfur-based ligands (usually thiols) [45] are needed for the formation of SAMs on noble metals, various approaches have been used to covalently bind AB-terminated ligands to silicon[50]–[53]. It's important to remember, however, that once

immobilized, the AB groups need enough space to isomerize—the volume needed for trans-to-cis switching of the parent AB unit is calculated to ~ 127 Å [54]. Though isomerization is not an issue for molecules moving freely in solution, it can be greatly reduced in closely packed monolayers—a challenge that has been thoroughly examined in SAMs on Au. Several groups studied the packing properties of self-assembled monolayers of simple alkyl AB thiols molecules on Au(111) in the mid-1990s(e.g., [55]–[57]). SPM experiments demonstrate that these molecules are densely packed on the surface, with a single molecule occupying an average surface area of 0.187 nm^2 [56] . As compared to this value, the average surface area occupied by single alkyl thiol molecule on Au is higher which is 0.215 nm^2 as revealed by Scanning Tunneling Microscope[58]. The interaction between AB groups in monolayer impacts packing density of monolayers, rather than by the underlying Au(111) substrate[59]. AFM and STM experiments show that the AB units in the SAMs are oriented in a herringbone pattern, with their short axes generally parallel to each other [55], [60]. With all of this in mind, it is no surprise that SAMs of AB thiols on Au were previously thought to be photochemically inactive [61], [62]. Multiple literature shows that in order to photoswitch AB-containing SAMs, the minimum surface area occupied by a single AB ligand should be 0.40 nm^2 [63], [64](only for planar substrates) as shown in Table 1.

Photoswitching of densely packed AB-SAMs are not significant as a result of steric hinderance or excitonic coupling; therefore, the chromophore density should be decreased[27], [28]. However, E. Titov et al. reported that azobenzene dimer in a close-packed environment show that the decreased trans–cis photoisomerization after $\pi\pi^*$ excitation is due to steric hindrance rather than excitonic coupling by molecular dynamics

simulations model system [65].

Table 1. Isomerization success in chosen nanocomponent SAMs of different AB thiols and average surface areas occupied by a single AB molecule.

Surface area occupied by a single molecule (nm^2)	Switching observed?	Ref.
0.19	No	[56]
0.25	No	[66]
0.26	No	[59]
0.30	No	[67]
0.31	No	[68]
0.39	No	[69]
0.41	Yes	[70]
0.43	Yes	[71]
0.50	Yes	[72]
0.66	Yes	[73]
0.75	Yes	[74]
0.87	Yes	[75]

Making mixed self-assembled monolayers (mSAMs) with an Azo-functionalized thiol and a shorter background ligand, serving as a spacer, is one way to build free volume necessary for isomerization (Fig 2). To elucidate the interplay between the switching property and

the microscopic structure of the mSAMs film, there have been several studies with scanning probe microscopy techniques[76]–[81]. mSAMs can be prepared by mixing a SAM composed of azobenzene-alkanethiolates (as switches) and alkanethiolates (as spacers) which requires that no phase segregation occurs between two molecules [14]. An asymmetrical disulfide comprising an azobenzene-alkanethiol and a simple alkane-thiol is one way to make mixed SAMs. The S–S link breaks upon adsorption on the surface, leaving two thiolates behind [29]. In these SAMs, photoisomerization was detected [29], [71], [82]. However, this approach only allows for a 1:1 mixing ratio in the preparation of SAMs. The production of a SAM from a mixed thiols solution is a more versatile technique [6]. It enables the azobenzene-containing thiolate content on the surface to be easily adjusted. Several studies have demonstrated the photoisomerization of mixed SAMs comprising azobenzene-functionalized thiols and alkanethiols [30]–[32] [79], [83]. However, in certain situations, the two thiols split into just one species' [84], [85]domains, or one species was completely displaced off the surface [86]. This is due to greater interactions between similar molecules than between different molecules, indicating preferential adsorption of a single species. If the azobenzene moieties interact significantly with them other, phase segregation may ensue. They observed near-statistical mixing and significant photoisomerization in mixed SAMs of an azobenzene-alkanethiol and a simple alkanethiol [87]. They assume that the lengthy alkyl chains in both molecules prevent the azobenzene-bearing thiol from adsorbing preferentially [14].

2.4 Self-Assembled Monolayers on Template Stripped Gold:

I discussed Self-Assembled Monolayers on a surface of Solid Substrate in the preceding section. Self-Assembled Monolayers on metal (gold) and semiconductors have been studied in several articles[24], [47]–[49] [50]–[53][54][55]–[57]. Gold was chosen because it forms a strong covalent bond with the thiol (-SH) headgroup found in most of the molecules in the research. In comparison to other metals such as silver and copper, it is also an inert metal [45]. Because of this feature, it may be used to handle and manipulate samples in ambient air rather than ultra-high vacuum [88]. Past research has used different process for the preparation of Self-Assembled Monolayers on this gold substrate such as evaporation of gold on mica sheet, evaporation of gold on glass, and TSG using mica sheets[24], [35], [45], [89]–[92]. However, there has not been a lot of work done on Self-Assembled Monolayers on Template Stripped gold[35], [89], [90], [92]. In this work, I am using template stripped gold on Si/SiO2.

2.5 Isomerization of AB bearing-Self-Assembled Monolayers by Scanning Tunneling Microscope:

Isomerization such as by resonant or inelastic tunneling of electrons[93], [94], [95] and electric field [20], [34] other than photoisomerization by using Scanning Tunneling Microscopy has been investigated before. Wen, Jin et al. has investigated the electric field switching of azobenzene containing self-assembled monolayers by theoretical calculation[34]. Besides this, there is one experimental work regarding the electric field switching of 3,3′,5,5′-tetra-tert-butylazobenzene(TBA) using Scanning tunneling microscope[20].

2.6 Excitonic Coupling:

When a material absorbs a photon with higher energy than its band gap, a pair of an electron and hole being bound to each other by Coulomb force. This pair is called exciton. Excitons can be categorized according to their binding energy and the dielectric constant of the surrounding medium (see, for example,[96]): Inorganic semiconductors with a high dielectric constant include Wannier excitons. They generally have a binding energy of less than 0.1 eV and span over many lattice sites. On the other hand, Frenkel excitons, are localized at a single lattice site and arise in materials with a low dielectric constant, such as molecular and ionic crystals. They have up to 1 eV binding energies. Because a SAM is a two-dimensional molecular crystal, excitons in SAMs are Frenkel excitons.

The wave functions of neighboring molecules' border orbitals do not overlap appreciably in molecular crystals. As a result, the molecules mostly interact by van der Waals forces. Nonetheless, in a crystal, the excited states of the molecules interact with one another. The exciton produced by photon absorption may be localized at a single lattice site or delocalized across several lattice sites, depending on the oscillator intensity of the optical stimulation and the intermolecular distance. A. S. Davydov mathematically described this phenomenon, which is known as excitonic coupling [97].

3. SAMPLE PREPARATION

The chapter describes the method used to prepare the samples. The corresponding working recipes is outlined in detail. We begin with the preparation of Template Stripped gold on Si/SiO2. The process for the preparation of Self-Assembled Monolayers of Azobenzene-thiol (Az11) is extensively explained. The spacer chain, which we used here is 1-decanethiol (C10), is mixed with Az11 to make mixed Self-Assembled Monolayers of Az11 and C10 (see Figure 3). The techniques to characterize these samples is discussed in next chapter. The sample preparations are done in the RFM 2234.

3.1 Template Stripped Gold

3.1.1 E-beam Evaporation of Gold on Si/SiO2 wafer

Electron beam evaporation is a physical vapor deposition technique employed for thin film coatings. As we need ultra-flat surface of Silicon, we use prime grade wafer (n-type, As doped, resistivity:0.001-0.005 ohm-cm, orientation:100, 4 inch diameter) purchased from University Wafer.

The evaporator we use is Angstrom Engineering EvoVac available in SRO inside NRSC cleanroom as shown in Figure 6. There is a Quartz Crystal Monitor to monitor the thickness of the deposited material. Figure 4 depicts the schematic for the e-beam evaporator process. Using a transfer chamber, the silicon wafer is put into the e-beam chamber. The power is now applied to the gold-containing crucible, and it is steadily raised until the gold begins to evaporate. The gold evaporates, creating a build-up of vapor pressure in the chamber. In a vapor stream, the evaporated gold passes through the chamber and collides with the silicon wafer substrate, producing a coating. When the evaporation process begins, the

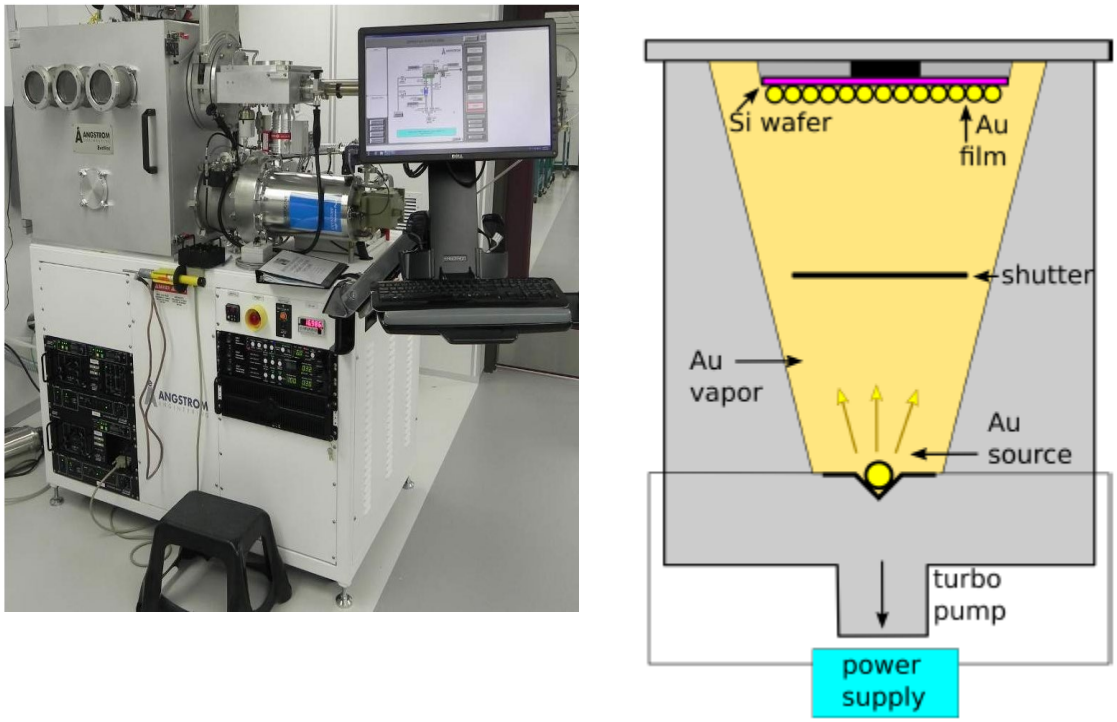

Figure 6: Angstrom Engineering EvoVac E-beam Evaporator and Schematic for the e-beam evaporator process [98].

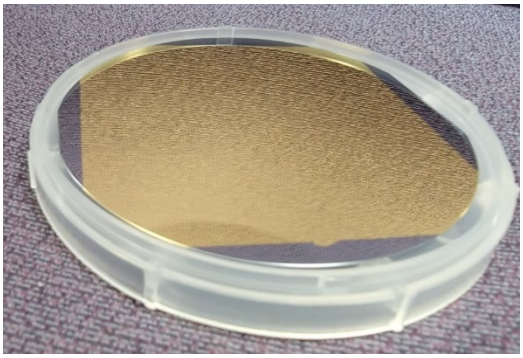

Figure 7: E-beam evaporated Gold with thickness of 100 nm on Si/SiO2

shutter is closed to ensure that any contaminants that fall off the evaporation boat do not land on the sample. When the substrate is ready for deposition, the shutter opens. We can

increase our power to speed up the deposition process. With a deposition rate of 0.5 Å/sec, 100 nm gold is deposited on the silicon wafer as shown in Figure 7. The evaporation is done here at a pressure about 10^{-7} Torr.

3.1.2 Template Stripped Gold (TSG)

The roughness of deposited gold on silicon by evaporation and sputtering is higher than template stripped gold[89]. Thus, we used TSG as our substrate. Now, we will discuss about the process to make TSG as we go further along which is shown in Fig 8.

Instead of using the top of the gold that was lastly deposited during evaporation, template stripping gold utilizes the bottom of the gold film, which is the gold that is touching the surface of Si/SiO2 substrate. Support structures must be attached to the top of the silicon substrate in order to transfer the gold from it. Another silicon wafer was diced using diamond cutter into small coupons (3-6 mm by 5-7 mm). We ultrasonicated these small coupons for 5 minutes with acetone, ethanol, and isopropyl each.

As the adhesive layer, 2 uL of thermally curable epoxy resins (two components, Epoxy Technology, EPO-TEK® 377) were dropped onto cleaned tiny silicon coupons (3-6 mm by 5-7 mm) using a micropipette. As illustrated in Figure 9, the glue-applied silicon coupons are bonded to the gold-deposited silicon wafer, producing a sandwich structure of Si/epoxy/Au//SiO2/Si. After that, we used an oven to bake the sandwich structure at 150ºC for one and a half hour in air. Figure. 9 and Figure. 10 shows the sandwich structure after it is baked. We should be careful with the amount of epoxy glue used in the coupons of silicon to avoid glue overflow. If there is an overflow of glue, neighboring bonded silicon coupons will stick together, making it impossible to remove when stripped.

Using a razor blade, the edges of an attached coupons are gently peeled and then tension is applied to a corner, causing the Si/epoxy/Au sample to pop off the substrate and allowing the gold to be template stripped as shown in Figure. 9 and Figure. 10.

The TSG sample was imaged with AFM in tapping mode using silicon tips (OPUS 160 AC-NA, MicroMasch, resonance frequency 300 kHz, force constant: 26 N/m, length: 160um) to measure the roughness and topography, as shown in Figure 11.

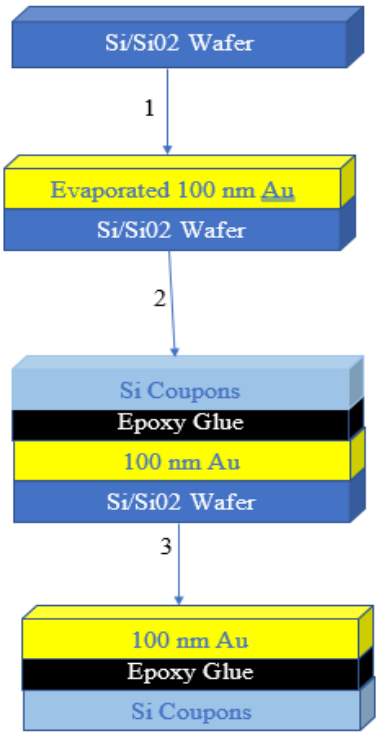

Figure 8: Schematic of Template Stripping (TSG) Process 1) Deposition of 100 nm Au on Si/SiO2 wafer using e-beam evaporator, 2) Applying epoxy glue on Si coupons and place it on the Au deposited Si/SiO2 wafer, and 3) Stripped off the Au using razor blade resulting TSG (Au/epoxy glue/Si coupons)

The typical free oscillation amplitude and amplitude set point is 20 nm and 20000.The root mean squared roughness of 5 um by 5 um and 0.5 um by 0.5 um scan area are R_s =

681.9 pm and R_s= 378.6 pm, respectively. We can see the atomic steps of gold in the TSG sample, too.

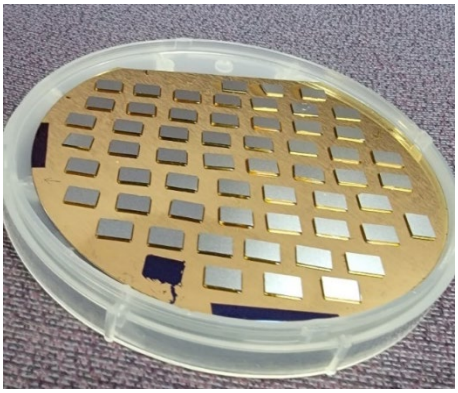

Figure 9: Sandwich structure of Si/epoxy/Au/Si/SiO2 with different sizes coupons (3-6 mm by 5-7 mm)

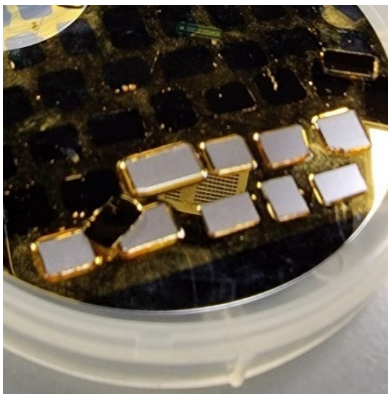

Figure 10: Sandwich Structure of Si/epoxy/Au/Si/SiO2 after scrapping off gold**.**

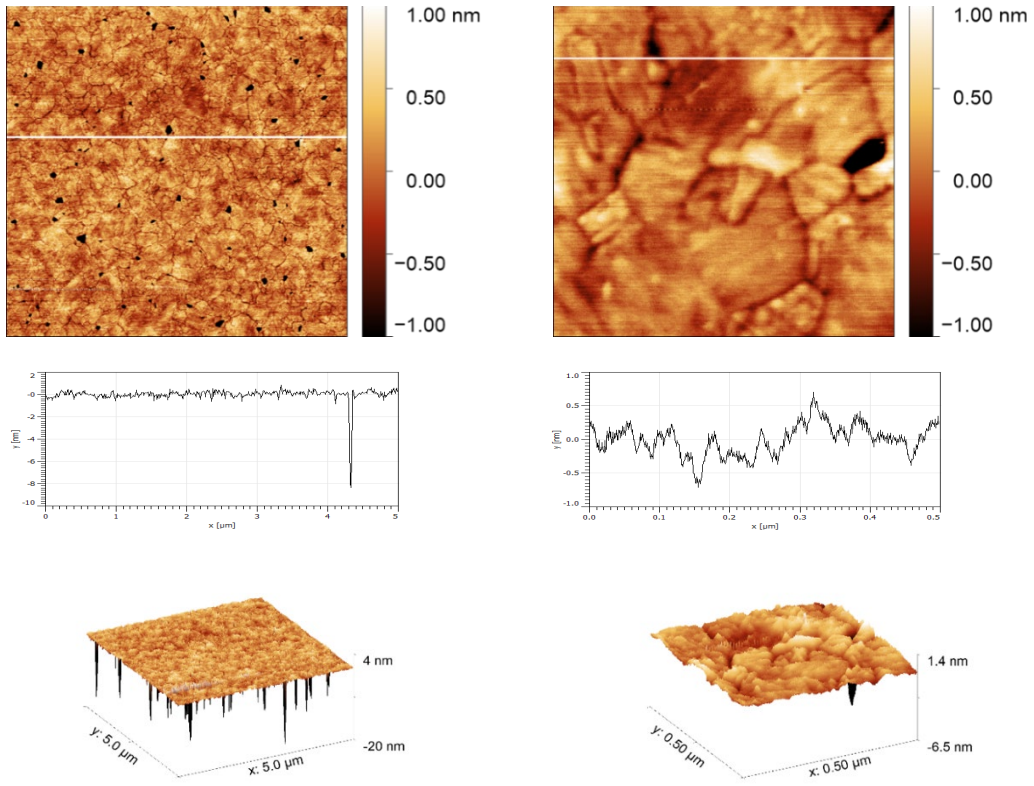

Figure 11: Tapping Mode-AFM images of TSG in air by AIST-NT AFM. The left images show 5um by 5um scan area and the right images shows 0.5um by 0.5um scan area of the same sample. A grey line indicates the line profiles in the AFM images.

3.2 Preparation of Mixed Self-Assembled Monolayers (mSAMs) of Azobenzene-thiols (Az11) and Decane-thiols (C10):

First, we prepared Self-Assembled Monolayers of Az11 by submerging freshly cleaved TSG substrate in an ethanol solution of Az11 and then we prepared Self-Assembled Monolayers of C10 by submerging freshly cleaved TSG substrate in an ethanol solution of C10 for half an hour to 24 hours. Then, we mixed these solutions by some proportions and submerge fresh TSG to prepare mixed Self-Assembled Monolayers

of Az11 and C10. These mSAMs will be characterized using Fourier Transform Infrared Spectroscopy, Atomic Force Microscopy, Kelvin Probe Force Microscopy later.

3.2.1 Solution preparation of Az11 and C10 and Incubation:

This section explains how to make 50 mL of a 1mM Az11 and C10 solution. Using the Sartorius, A-7073 -03 400,000 g scale, we determined the mass necessary to achieve a concentration of 1mM of Az11 (0.019 grams). Dr. Bill Britain's group produced azobenzene-thiol (Az11) in his lab. Now, we added ethanol solution (PHARMCO by Greenfield Global, (NLT (no less than) 99.5% ethanol, 0.2% max water)) and ultrasonicated for 10 minutes to get a transparent 50mL Az11 solution with a concentration of 1mM, as shown in Figure12a)).

We used 50 mL of 1-decanethiol 96% purchased from Sigma-Aldrich (Density = 0.824 g/mL at 25 °C (lit.)) to make 50mL of C10. From this density, we estimated the concentration, which is about 4.72 M. We produced a C10 solution with a 1mM concentration by taking 11uL of this solution and mixing it with 100 percent ethanol solution using a micropipette (Figure12 b)).

After making 1mM Az11 and C10 solutions, I made binary incubated solutions by changing the volume of two components (Az11, C10). We utilized concentrations of Az11 of 1 percent, 10 percent, 20 percent, 50 percent, and 100 percent by volume in this study.

As illustrated in Figure 13, the incubation solution is next added to a 5mL tube. A freshly cleaved TSG substrate is subsequently submerged in an upright position in the tube (Figure 13.). The incubation is kept out of UV rays by keeping it in a dark area or covering it in aluminum foil. After the required incubation period, the sample is removed and rinsed with

500 mL of ethanol for 30 seconds using a spray bottle. After that, high-pressure nitrogen is used to blast it dry. The whole process is illustrated in Figure 14.

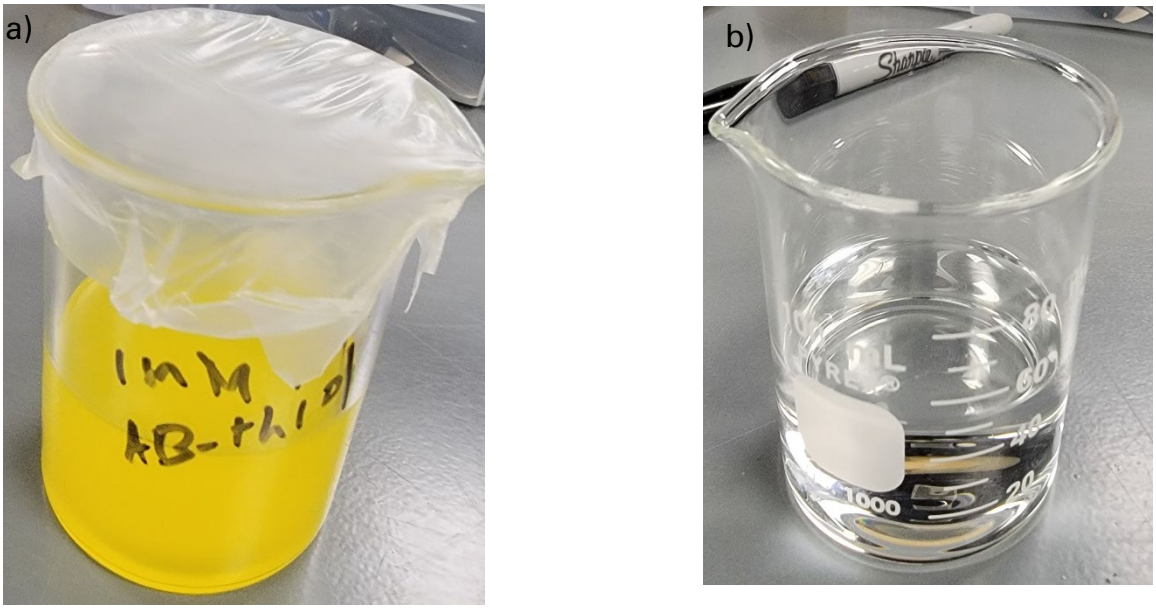

Figure 12: a) 1mM solution of Az11 and b) C10 after ultrasonication.

The stock solutions, which is prepared in 50 mL, is kept by wrapping it with Parafilm M and aluminum foil for future incubations at room temperature. We ultrasonicated for 5 minutes every time we utilized this stock solution to produce mSAMs, since there is precipitation of the Az11 particles which we assume the solid residue from disulfide. We use Parafilm M to effectively encapsulate the ethanol containing Az11. To utilize this stock solution of C10, we follow the same method as we did with the prior stock Az11 solution because ethanol is volatile.

3.2.2 Incubation Time:

We varied the incubation time ranging from 30 minutes to 24 hours. And we found that the incubation time longer than 1 hour, the submerged TSG substrate forms bubbles due to the penetration of the solution through the defects in the TSG film. Here, we noted that the gold silicide formation is most likely the cause of the defects in the TSG, but it is still under investigation. Therefore, we chose 1 hour incubation time for all samples. This will be discussed more in the result section.

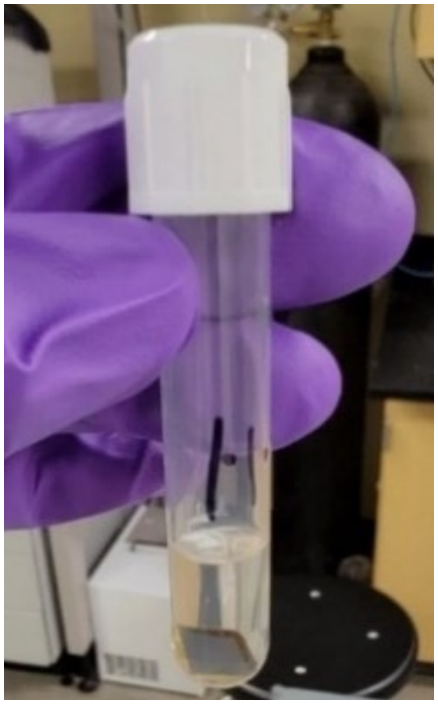

Figure 13: TSG substrate submerged in the solution containing 1% Az11 and 99% C10 for 1 hour.

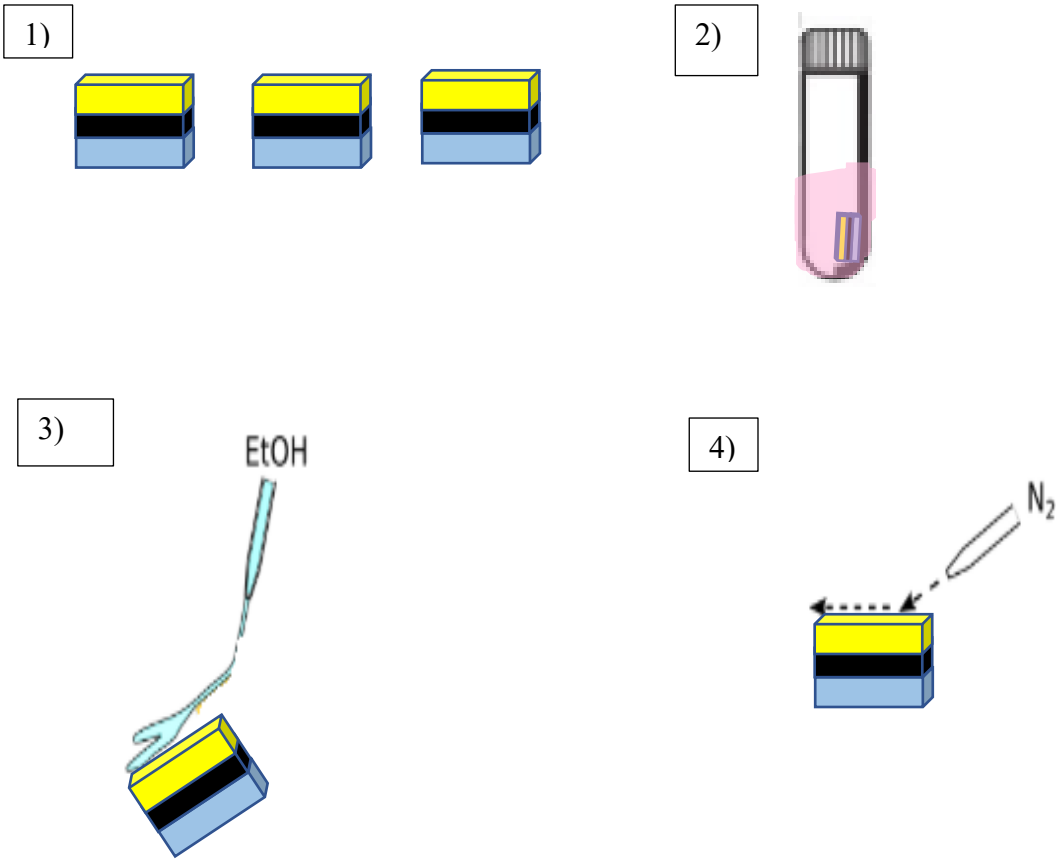

Figure 14: Schematic diagram of process of making mixed Self-Assembled Monolayers 1) cleaving TSGs, 2) incubation, 3) rinsing, 4) Blow drying [98].

3.3 Characterization of Mixed Self-Assembled Monolayers:

We will use Fourier Transform Infrared Spectroscopy (FTIR) and Atomic Force Microscopy, Kelvin Probe Force Microscopy to characterize our mixed Self-Assembled Monolayers. Figure 15. shows the cartoon illustration of mixed SAMs on TSG and the molecular sketch of C10 and Az11 in mSAMs.

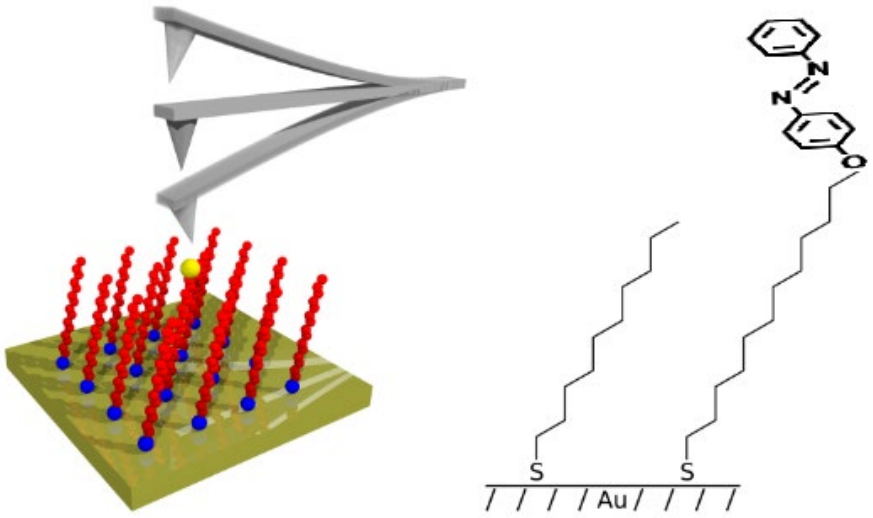

Figure 15: Left shows the cartoon illustration of mixed Self-Assembled Monolayers on TSG surface, where the red chain represents the alkane chains (C10), blue sphere represents the sulfur attached to the gold surface and yellow sphere on the top of alkane chain represents an azobenzene molecules. Here, Cantilever is not drawn to scale. Right shows the molecular sketch of C10 and Az11 on TSG[98].

The typical example of AFM topography image (1 um by 1 um scale) and line profile of 10% Az11 and 90% C10 mSAMs is shown in Figure 16. Here, we use Tapping-Mode AFM to get the topography of the sample. We see a lot of small blobs distributed across the surface. The height of these blobs is approximately 1nm, which we suggest that this is the head group of Az11. To make sure that these blobs are Azobenzene molecules, we will get the topography images after UV irradiation, which will be discussed in result section. After exposure with UV wavelength, we will apply electric field to the sample using AFM tip. The result will be discussed in the result section.

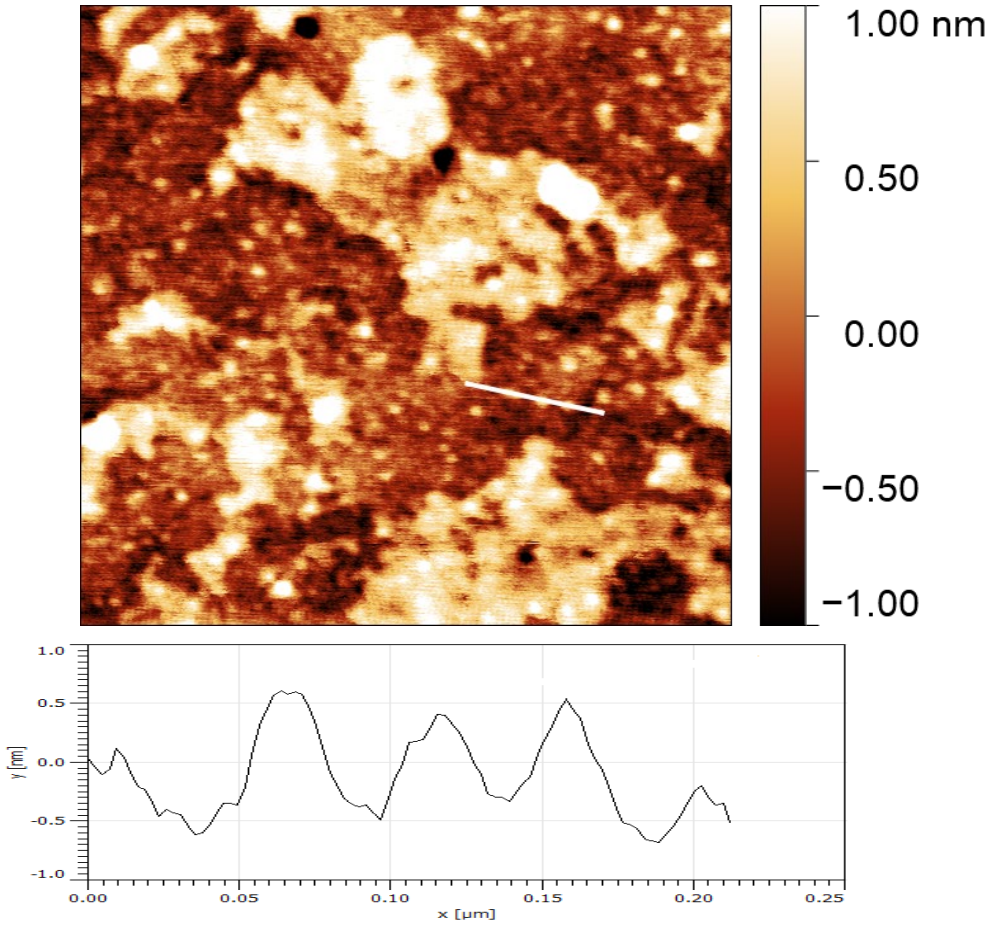

Figure 16: Tapping-Mode AFM image in air (1 um by 1um scale) and Line Profile of mixed Self-Assembled Monolayers (mSAMs) of 10% Az11 and 90% C10.

4. EXPERIMENTAL TECHNIQUES

We have already explained how to prepare the Azobenzene-containing mixed Self-Assembled Monolayers on TSG/Si/SiO2. Now, we aimed to describe our sample using multiple techniques such as Fourier Transform Infrared Spectroscopy, Atomic Force Microscopy, and Kelvin Probe Force Microscopy based on previous research. This chapter delves into the theory and design of these methods.

4.1 Fourier Transform Infrared Spectroscopy (FTIR)

FTIR is used to identify species present on the surface. Here, we use diamond ATR crystal to characterize Azobenzene containing mixed Self-assembled monolayers on top of Template Stripped Gold on Si/SiO2 surface. In this work, I have used BRUKER ALPHA II FTIR SPECTROMETER, which is on RFM 2226, ARSC, Texas State University. The setup to mount the sample is shown in Figure.17.

When this instrument is ready, we clean the ATR diamond crystal with soft tissues using alcohol. Then, we take a background spectrum. After that, we place the sample on top of the crystal (2mm in diameter) and clamped it using an anvil to ensure that the sample receives the proper contact pressure.

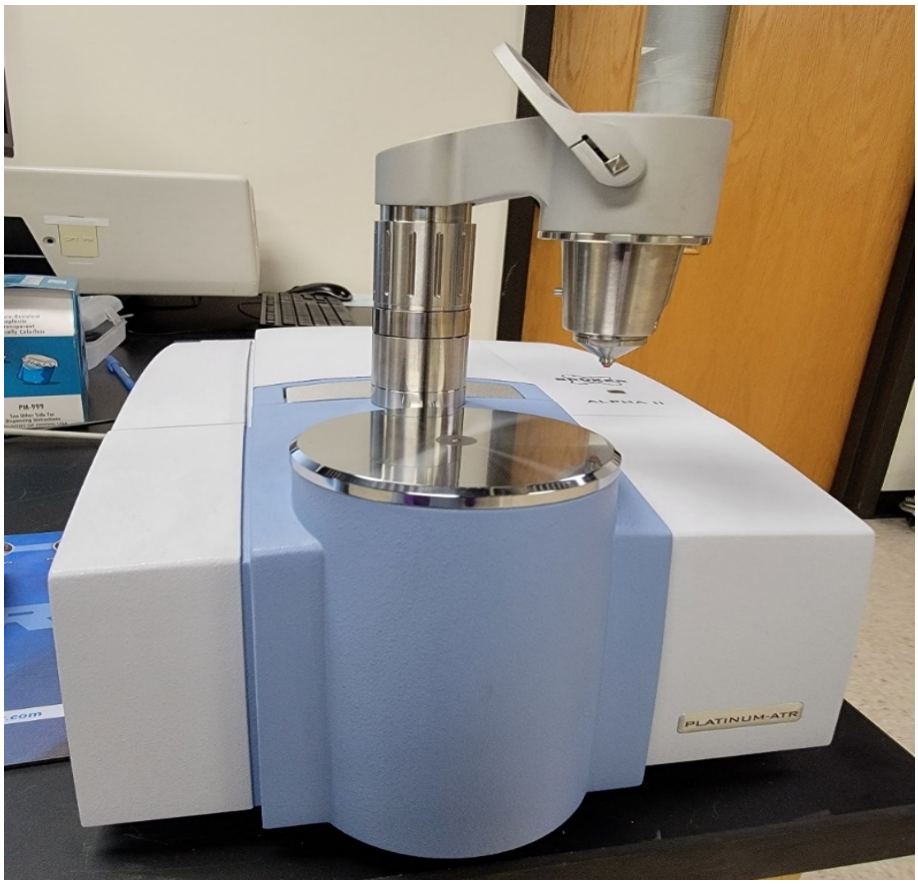

Figure 17: Bruker ALPHA II FTIR spectrometer**.**

4.1.1 Working Principle of FTIR

A. A. Michelson revolutionized spectrometry when he designed a two-beam interferometer in 1891. Almost all infrared spectrometers in use today have an interferometer (FTIR spectrometers). Two mirrors, one fixed and one moveable, with a beam splitter, make up the Michelson interferometer. A source generates an infrared beam controlled by mirrors through the interferometer, spectrometer, and onto the sample

compartment before reaching the detector. After that, the detected signal (also known as an interferogram) is Fourier Transformed to produce a spectrum. The name of this spectrometric (FTIR)[99] approach comes from this computation. The intensity of the signal which reaches the detector depends on the absorption of the infrared beam when interacting with the sample. All molecules have a certain natural vibrational frequency. When a molecule is illuminated with infrared radiation of the same frequency as that of the molecule, the infrared radiation may be absorbed by the molecule. The molecule is only able to absorb infrared radiation of the same frequency as its natural vibrational frequency. If the dipole moment of the molecule varies during the vibration, the molecular vibration is infrared active. As a result, when a molecule is irradiated with infrared light of various frequencies (as in a spectrometer), it will selectively absorb light with a frequency corresponding to the molecule's natural vibrational frequency, as shown in Figure. 17. When a molecule absorbs infrared light, it transitions from one vibrational energy state to another, increasing its own vibrational energy and vibrating with greater amplitude[100]. Stretching and bending modes of molecular vibrations are two major modes of molecular vibrations employed in this study. Variations in the bond length between the atoms in the molecule describe the former, whereas changes in the bond angle between the atoms indicate the latter. The strength of the signal that reaches the detector is reduced when infrared light is absorbed by the sample.

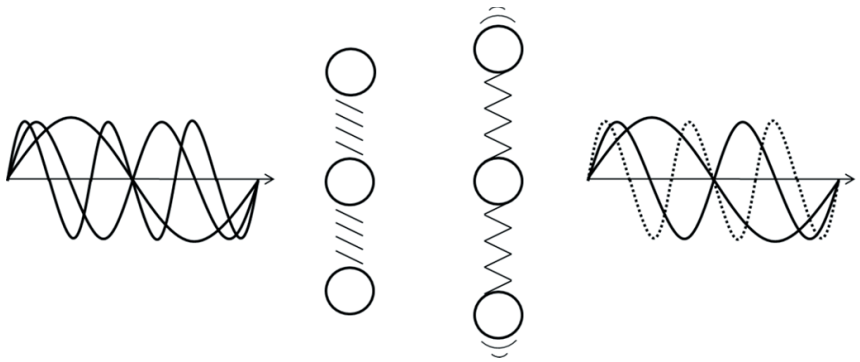

Figure 18: Schematic figure illustrating absorption of before (left) and after infrared radiation(right)[101] .

4.1.2 The Attenuated Total Reflectance (ATR) Technique

Internal reflection is used in the attenuated total reflectance (ATR) approach, in which the infrared beam is completely reflected within an ATR crystal[102], as shown in Figure 4. The ATR crystal must have a higher refractive index (n_1) than the sample to accomplish complete reflection (n_2). When the angle of incidence is greater than the critical angle, total reflection occurs. The angle of incidence is the angle measured with respect to the normal and the critical angle is measured according to [102],

$$\theta_{\text{critical}} = \sin^{-1}\left(\frac{n_2}{n_1}\right) \tag{3}$$

An evanescent wave from the infrared beam is formed perpendicular to the surface of the ATR crystal at each point of reflection, as shown in Figure 13. The evanescent wave's electric field interacts with the sample near the ATR crystal, with parts of the electric field being absorbed by the sample, resulting in attenuation in the intensity of the reflected infrared beam, hence the technique's name. The amplitude of the electric field is decreased exponentially with the distance of the surface, z, of the ATR crystal as,

$$E = E_0 e^{-z/d_p} \tag{4}$$

Here, E and E_0 are the electric fields after and before exponential decline. d_p is the penetration depth (typically around some hundreds of nanometers to a few micrometers), which measures how far will the Electric field reaches from the surface of the ATR crystal.

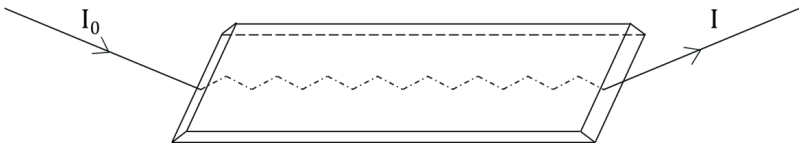

Figure 19: Schematic diagram of ATR technique, where I and I_0 are the intensities of the infrared beam after and before interaction with the sample [101].

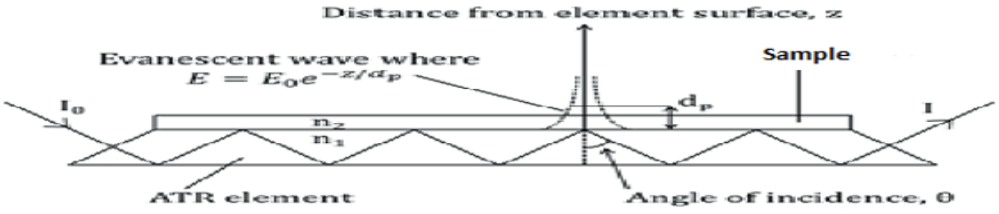

Figure 20: Schematic diagram representation of ATR technique where evanescent wave is penetrating the sample [101].

The penetration depth can be approximated as[102],

$$d_p = \frac{\lambda}{2\pi(\sin^2\theta - n_{21}^2)^{1/2}} \quad (5)$$

Here, λ is the wavelength of the infrared radiation inside the ATR crystal, θ is the angle of incidence, and n_{21} is the ratio of refractive indices.

4.2 Atomic Force Microscopy

The atomic force microscope (AFM) has been a common instrument in nanotechnology since its invention in 1986 [103]. There are three operating modes of AFM which are contact, non-contact, and tapping. In all three modes, the contact forces between the tip and sample can be clearly detected on a force–displacement curve, as illustrated in Figure. 21. Weak attractive forces are formed between the tip and the sample when the interatomic distance is considerable. The attraction forces between the atoms build as they are brought closer together, until the atoms are so near that the electron clouds begin to resist each other electrostatically. As the interatomic distance shrinks, the repulsive force between the atoms reduces, weakening the attractive forces. When the distance between the atoms approaches a few Angstroms, the interaction force approaches zero, and when the atoms are in touch, it becomes entirely repulsive.[104]

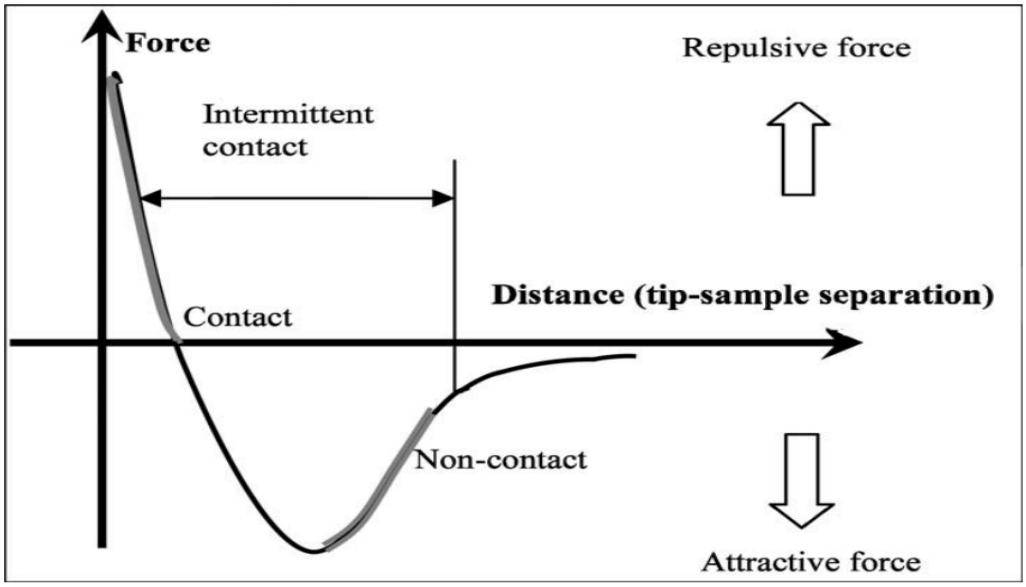

Figure 21: Variation in interatomic force as a function of sample distance from AFM tip [104].

A sharp tip at or near the end of a micro-structured cantilever characterized the sample surface in direct mechanical contact to measure the force acting between tip and sample in contact mode as shown in Figure.21. We can get sample's topography, which are the maps of constant tip-sample interaction force, by maintaining cantilever deflection constant. This is done by a feedback loop that continually changes the sample's z-position during the scan process so that the deflection sensor's output remains constant at a predetermined set-point [105]. Because of the lateral forces acting between tip and sample, the resolution is limited in contact mode especially for soft samples. Therefore, it is preferable to vibrate the cantilever vertically near the sample surface to eliminate this effect. This AFM technique which uses oscillating cantilever to image a sample's surface is called Dynamic Force Microscopy (DFM) [106].

Non-contact mode allows for non-invasive and very precise topographical photography by oscillating at the attractive force regime in close proximity to the surface without touching the sample [107].

A vibrating cantilever is kept at a tip-to-sample distance near to the area of the force–distance curve used by contact mode in the tapping mode. The vibrational movement of the cantilever at its lowest point simply contacts or taps the surface as shown in Figure. 22 The changes in the cantilever's vibrational parameters are monitored when the sample is raster-scanned underneath the tip, and the feedback parameters adjustment employed to maintain these parameters constant is processed to provide a topographical image.[108] This method is preferred to get high resolution images.[104]

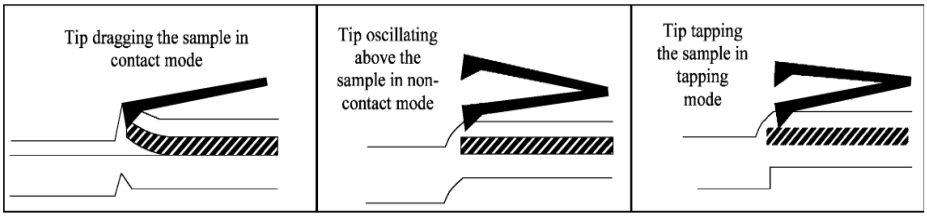

Figure 22: Contact Mode (left), non-contact mode (middle), and tapping mode (right) [104].

4.2.1 Experimental Setup and Theory of Tapping Mode-Atomic Force Microscopy

The experimental setup of tapping mode is shown in Figure 23. The cantilever's resonant frequency (and hence amplitude A and phase ϕ) varies with the tip-sample distance (d) due to the tip–sample interaction. As a result, either the amplitude or phase may be employed for the distance feedback control. The amplitude, for example, is supplied as a set-point, and the feedback loop adjusts the tip–sample distance to keep the amplitude constant. The scanned height effectively depicts the surface topography, and the tip-sample distance is a function of the tip's lateral position with respect to the sample. The laser beam deflection technique is commonly used to determine the cantilever's deflection. The cantilever is driven with a set frequency and constant excitation amplitude by an external function generator in traditional tapping mode, and the ensuing oscillation amplitude and/or phase shift are monitored by a lock-in amplifier[105].

The AFM we used in this is ARSC AIST-NT Atomic Force Microscope (AFM) which is in RFM 1202, Texas State University as shown in Figure 24.

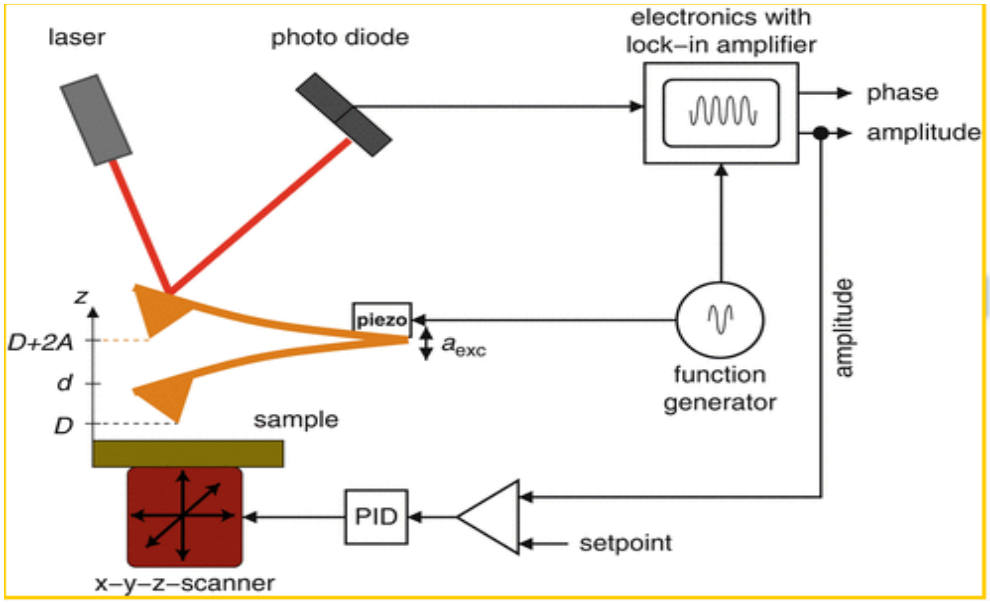

Figure 23: Schematic diagram of Tapping Mode- AFM[105].

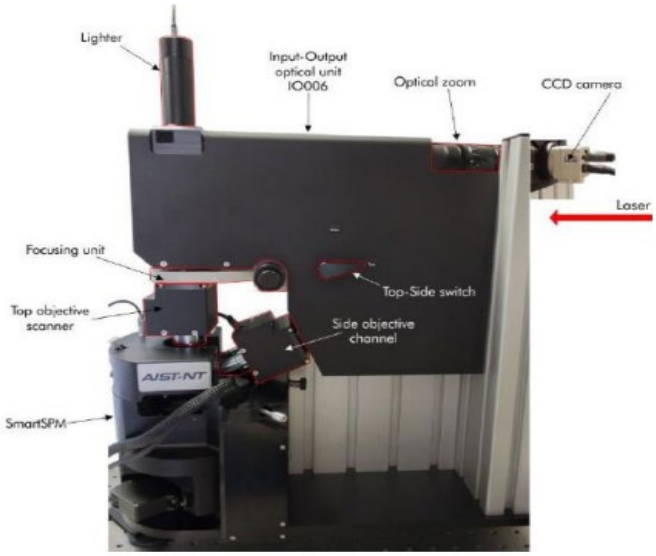

Figure 24: ARSC AIST-NT AFM**.**

4.3 Kelvin Probe Force Microscopy

Kelvin probe force microscopy, which is based on the Kelvin probe concept, is used to detect the surface potential using the AFM in noncontact mode[109]–[111].

Electrons move from the lower work function material to the higher work function material when the tip and sample are electrically linked (Figure 1). The following equation gives the value of this contact potential difference (V_{CPD}):

$$V_{CPD} = (\phi_{tip} - \phi_{sample})/-e \quad (6)$$

Here, ϕ_{tip} and ϕ_{sample} are work functions of the tip and sample, and e is the magnitude of the charge of electron. Because the contact potential difference is sensitive to adsorbed molecules on the surface and the existence of different phases within a material, it gives material contrast information[112], [113].

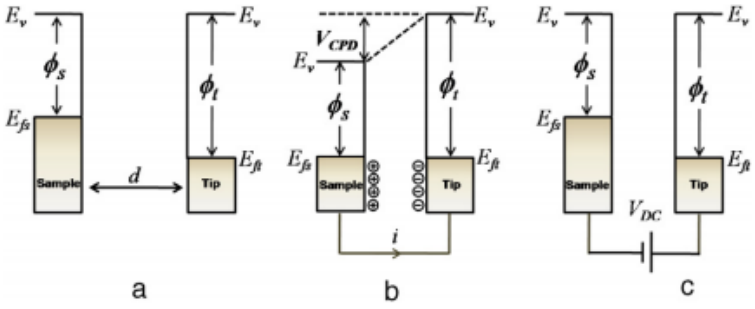

Figure 25: Electronic energy levels of the sample and AFM tip for three cases: (a) tip and sample are separated by distance d with no electrical contact, (b) tip and sample are in electrical contact, and (c) external bias (V_{dc}) is applied between tip and sample to nullify the CPD and, therefore, the tip–sample electrical force. E_v is the vacuum energy level. E_{fs} and E_{ft} are Fermi energy levels of the sample and tip, respectively[113].

KPFM assesses the work function of the sample by applying an AC voltage (V_{AC}) and a DC voltage (V_{DC}) to the AFM tip. V_{AC} produces oscillating electrical forces between the AFM tip and the sample surface, whereas V_{DC} cancels out the oscillating electrical forces caused by CPD. Between the AFM tip and the sample, the electrostatic force (F_{es}) is

calculated as follows:

$$F_{es}(z) = -\frac{1}{2}\Delta V^2 \frac{dC(z)}{dz} \tag{7}$$

Here, where dC/dz is the gradient of the capacitance between tip and sample surface, V is the potential difference between V_{CPD} and the voltage delivered to the AFM tip, and z is the direction normal to the sample surface. The voltage differential V will be when $V_{AC}\sin(\omega t) + V_{DC}$ is supplied to the AFM tip:

$$\Delta V = V_{tip} \pm V_{CPD} = (V_{DC} \pm V_{CPD}) + V_{AC}\sin(\omega t) \tag{8}$$

It is worth noting that the sign changes depending on whether the bias (VDC) is applied to the sample (+) or the tip (−)[114]. From

$$F_{es}(z,t) = -\frac{1}{2}\frac{\partial C(z)}{\partial z}[(V_{DC} \pm V_{CPD}) + V_{AC}\sin(\omega t)]^2 . \tag{9}$$

$$\Rightarrow \; F_{es}(z,t) = F_{DC} + F_{\omega} + F_{2\omega} \tag{10}$$

Here, $F_{DC} = -\frac{\partial C(z)}{\partial z}\left[\frac{1}{2}(V_{DC} \pm V_{CPD})^2\right]$, the DC force

$F_{\omega} = -\frac{\partial C(z)}{\partial z}(V_{DC} \pm V_{CPD})\, V_{AC}\sin(\omega t)$, a harmonic force with the same frequency of the AC tip bias (the first harmonic)

$F_{2\omega} = \frac{\partial C(z)}{\partial z}\left(\frac{1}{4}\right)V_{AC}^2[\cos(2\omega t) - 1]$, a harmonic force at double the frequency of the AC signal (the second harmonic)[112], [113]

There are two operational modes in KPFM: Amplitude-Modulation and Frequency Modulation[113]. Here, we use Frequency Modulation-KPFM.

4.3.1 Frequency Modulation- Kelvin Probe Force Microscopy:

F_{ω} is detected by the frequency shift at ω in FM mode KPFM, and V_{DC} is applied to the AFM tip to cancel the frequency shift, allowing V_{CPD} to be measured. In the FM-

KPFM mode, the frequency shift of the cantilever oscillation is used to detect the electrostatic force gradient, which improves spatial resolution. A schematic representation of a KPFM experimental equipment is shown in Figure 26. The FM mode AFM system for topographical measurement is shown in the lower section, while the components for CPD mapping, including the KPFM controller and lock-in amplifier, are shown in the upper half. The AM and FM mode KPFM setups are shown in the diagram by the dashed line and bold straight line. The lock-in amplifier reference signal voltage output provides V_{ac} to the tip (OSC out). The frequency shift signal (Δf) is divided in two in FM mode, with one going with the same frequency as V_{ac} is extracted by the lock-in amplifier and sent into the KPFM controller. By delivering V_{dc} to the tip, the KPFM controller maintains feedback to negate the lock-in output signal[113]. We performed the FM-KPFM measurements with the modified JEOL AFM (JSPM-52000) in our lab.

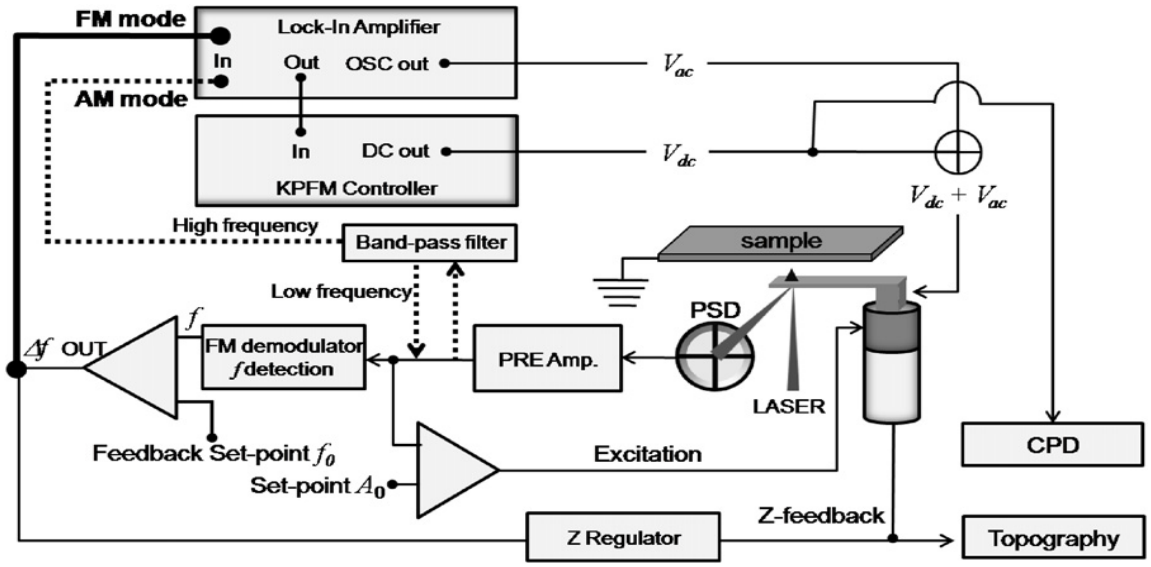

Figure 26: Schematic diagram of KPFM system showing AM and FM mode. Lower part of the diagram is an FM mode AFM system for topography imaging and upper part is a KPFM system for CPD measurement[113].

5. RESULTS

This thesis employs a variety of complementary methodologies to investigate molecular switches in SAMs. Fourier Transform Infrared Spectroscopy allows us to explore the chemical composition of SAMs. Tapping Mode in Atomic Force Microscopy allows us to study the morphology of the AB functionalized mSAMS before and after UV-radiation illumination. The differences between the surface potential before and after UV exposure of mSAMs on TSG on top of Si/SiO2 can be characterized by Kelvin Probe Force Microscopy (KPFM). When the local electric field is applied by AFM tip to the sample, we expect to observe reversible E/Z isomerization by measuring topography and surface potential using Tapping Mode AFM and KPFM.

5.1 Atomic Force Microscopy of Template Stripped Gold:

The sample preparation chapter explains how to make a template stripped gold. The topography of a template stripped gold substrate is discussed here. Our objective is to obtain a gold substrate as flat as possible. As a result, we tried several slightly different preparation protocols to improve template stripped gold, which are not included in the sample preparation chapter.

When we try to make TSG with etched SiO2 from Au deposited Si wafer, the bonding between the Si-Au is strong. We etched native oxide on Si wafer by using Buffered Oxide Etch solution (contains 6:1 volume ratio of 40% NH_4F in water to 49% Hydrofluoric (HF) in water) to obtain atomically flat Si surface. Therefore, we could not cleaved the gold from Si wafer. This experiment was unsuccessful. The second process for the preparation of TSG is the same as we explained in the sample preparation chapter. In the third process,

we have tried to improve the flatness of gold surfaces by annealing the gold evaporated Si substrate for a one hour at 300ºC using 3-Zone Tube Furnace (Figure 27.) after we deposited the gold on Si/SiO2. A 3-Zone Tube Furnace (Location: NRSC RFM 1246, Model: Lindberg) is a furnace capable of flexible annealing or chemical vapor deposition at temperatures below 1000ºC. Here, we use manifold to process and/or purge gases (Argon, 4% H_2 and Ar, and N_2 (we used)) into the quartz tube.

Figure 27: NRSC 3-Zone Tube Furnace (Model: Lindberg)

The Tapping-Mode AFM images of unannealed and annealed template stripped gold in air is shown in Figure 28.

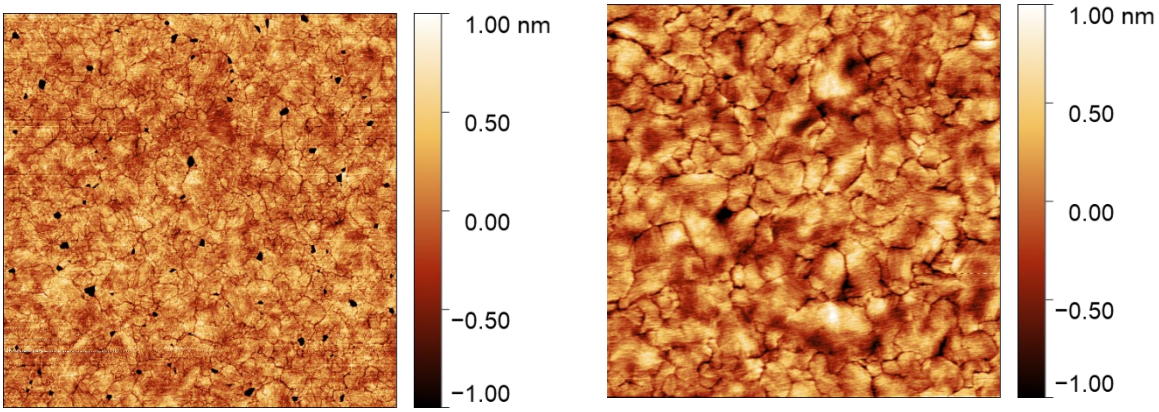

Figure 28: Tapping Mode AFM Images of unannealed TSG (left) and annealed for 1 hour at 300ºC TSG (right). Here both images are 5um by 5um scale taken in air.

The roughness (R_s = 301.7 pm) of annealed TSG is lower as compared to unannealed

TSG (R_s = 682.1 pm). The size of the grain is increased as you can see from AFM topography images shown in Figure 28. We have not used annealed TSG, for when we submerge this TSG in liquid more than 15 minutes, it starts to form bubbles, which we will discuss in the section 5.3.

5.2 Fourier Transform Infrared Spectroscopy (FTIR) of mixed Self-Assembled Monolayers (mSAMs)

The ATR FTIR was used in this work to confirm the absorption of Azobenzene moieties in mixed Self-Assembled Monolayers on TSG/Si/SiO2. The FTIR detection of mSAM absorption on TSG/Si/SiO2 is weak because mSAM is a monolayer film; therefore, we increased the mixing fraction of a 1 mM Azobenzene-thiol (Az11) solution and a 1 mM Decane-thiol (C10) solution from 1 to 50 using Azobenzene-thiol solution, which is discussed in detail in the sample preparation section. All the samples were incubated for 1 hour. FTIR spectra of the mSAM'S were recorded with the Bruker ALPHA II FTIR spectrometer at a resolution of 4 cm^{-1} with an average of 1000 scans. Figure 29. shows the FTIR spectrum of mixed SAMs of Az11 (10%, 20%, and 50%) and C10 on TSG, Template Stripped Gold/Si/SiO2, and Solid(neat) of Az11. We did not include the FTIR spectrum of mSAMs with 1% Az11 because we cannot see clear difference between 0% Az11 mSAM and 1% Az11 containing mixed SAMs.

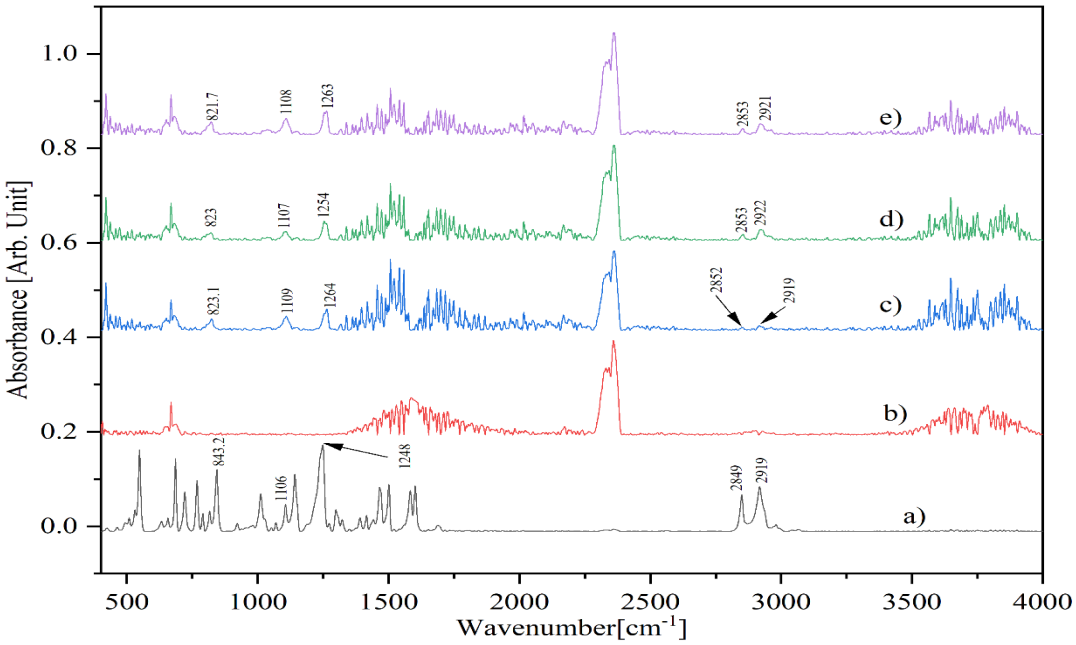

Figure 29: FTIR spectrum of a) Az11 neat (solid) b) Template Stripped Gold on Si/SiO2 (TSG) c) mixed Self-Assembled Monolayers of C10 (90%) and Az11(10%) on TSG d) mixed Self-Assembled Monolayers of C10 (80%) and Az11(20%) on TSG e) mixed Self-Assembled Monolayers of C10 (50%) and Az11(50%) on TSG.

Here, we can clearly see the differences in the TSG (b) and the mixed Self-Assembled Monolayers (c,d,e). Bands at 2919, 2849 for neat (solid) Az11; 2919, 2852 for mSAMs of C10 (90%) and Az11 (10%) on TSG; 2922, 2853 for mSAMs of C10 (80%) and Az11 (20%) on TSG; and 2921, 2853 for mSAMs of C10 (50%) and Az11 (50%) on TSG belong to the long aliphatic chain (considering 10% mSAM sample). The bands at 1248, 1106, 843.2 for neat (solid) Az11; 1264, 1109, 823.1 for for mSAMs of C10 (90%) and Az11 (10%) on TSG; 1254, 1107, 823 for mSAMs of C10 (80%) and Az11 (20%) on TSG; and 1263, 1108, 821.7 for mSAMs of C10 (50%) and Az11 (50%) on TSG correspond to

Azobenzene moieties, respectively.

Table 2. FTIR Data and Vibrational Assignment of Az11 in Neat Solid and Absorbed states on TSG.

Az11 Neat (solid) [cm^{-1}]	mSAMs of 10% Az11 [cm^{-1}]	mSAMs of 20 % Az11[cm^{-1}]	mSAMs of 50% Az11[cm^{-1}]	Assignment
2919	2919	2922	2921	$\nu_{as}(CH_2)$
2849	2852	2853	2853	$\nu_s(CH_2)$
1248	1264	1254	1263	$\nu_{as}(C0C)$
1106	1109	1107	1108	18b
843.2	823.1	823	821.7	10a out of plane

The peak locations of the symmetric and antisymmetric CH_2 stretching vibrations can be regarded as a sensitive indication of the alkyl chain ordering, according to previous work[115], [116], [76]. As we can see that the $\nu_{as}(CH_2)$ and $\nu_s(CH_2)$ modes in the mSAMs are observed in the higher frequencies than those in neat (solid) state, i.e., at 2919, 2922, 2921 and 2852, 2853's, in the Table 2 and at 2919, 2949 in the Az11 neat (solid) in the Table 2, respectively [76], [117]. This implies that the alkyl chains as well as azobenzene moieties are closely packed with an ordered conformation in neat Az11 (solid), while in the mSAMs the alkyl chains are disordered. The distinct peaks at 1248 in neat (solid) Az11 and 1264 in mSAMs of 10% AZ11, 1254 in mSAMs of 20% Az11, 1263 and

mSAMs of 50% Az11 can be attributed to $\nu_{as}(C0C)$ [76]. The peaks at 1106 in neat (solid) Az11 and 1109,1107, 1108 in mSAMs of 10%, 20% and 50% corresponds to 18b mode due to the presence of azobenzene in mSAMs [76], [118]. The bands at 843.2 in neat (solid) Az11 and 823.1, 823 and 821.7 belongs to out of plane benzene ring 10a mode (Figure 30.) [76],[118]. The observed lower frequency 10a mode in the mSAM is likely due to the interaction between Azobenzene moiety and surrounding molecules.

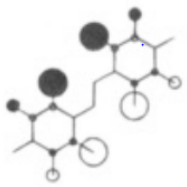

Figure 30: Calculated vibrational 10a mode of trans-azobenzene [118]**.**

5.3 Optical Images of the annealed and unannealed TSG Samples after submerging in Azobenzene-containing Solution:

In this section, we explain about the optical images of the annealed and unannealed TSG samples after submerging in Azobenzene-containing solution. The optical images were taken using Optical Microscope (Model: Olympus BX60M, Location: RFM 2226) as shown in Figure 31. This optical microscope has magnifications of 5-100X. Most of the optical images are taken in the magnifications of 10X. All the optical images shown here are annealed using the oven in our lab (HUMBOLDT, Model 20 GC Lab Oven) as shown in Figure 32. Figure 33. shows the optical images of 8 hour and 2 hour annealed TSG's and unannealed TSG sample.

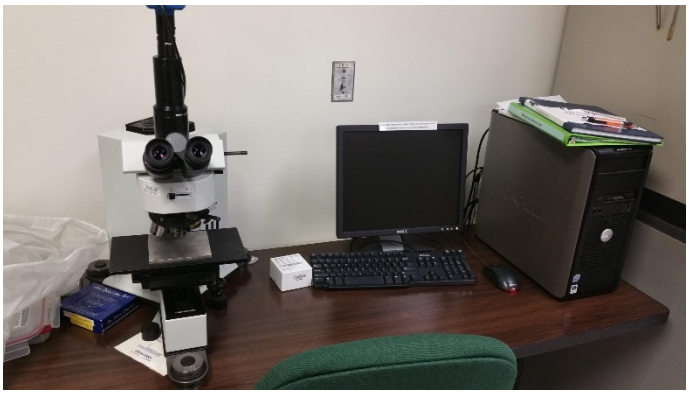

Figure 31: Optical Microscope (Model: Olympus BX60M).

Figure 32. Model 20 GC Lab Oven.

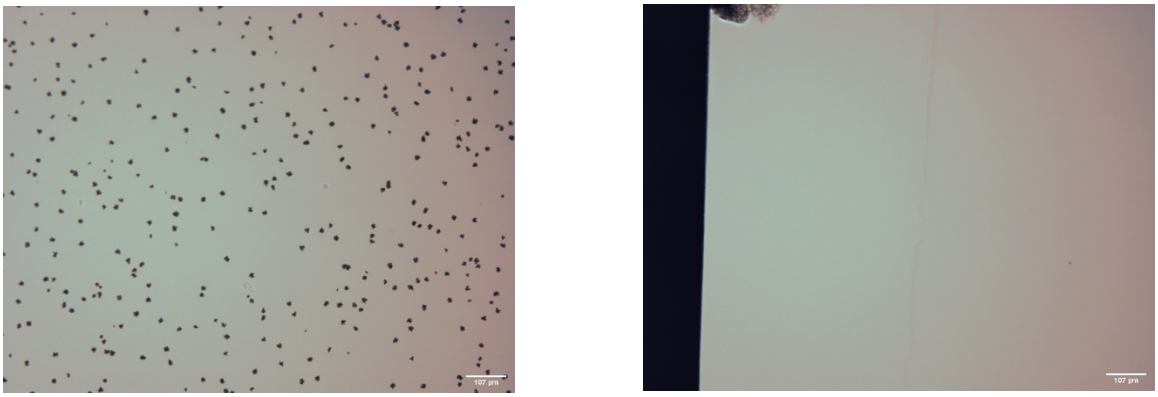

Figure 33: Optical Images of 8 hour annealed at (left) and unannealed TSG substrates (right).

We suggest that these black dots represent gold silicide formation when the gold diffuse

through the native SiO2 layer to Si. The gold silicide formation takes place at room temperature (25ºC) as suggested by these research articles in the absence of the interfacial SiO2 layer [119]–[121]. We have used unannealed TSG because when the TSG with gold silicides is submerged in the solution, the bubbles are formed around the gold silicides, which is shown in Figure 34. Also, Figure 34. shows the evolution of the bubbles through time which is submerged in ethanol solution (Time: 0 mins, 15 mins, 30mins). We can see clearly that the formation of bubbles starts from 15 minutes (Figure. 34 b)).

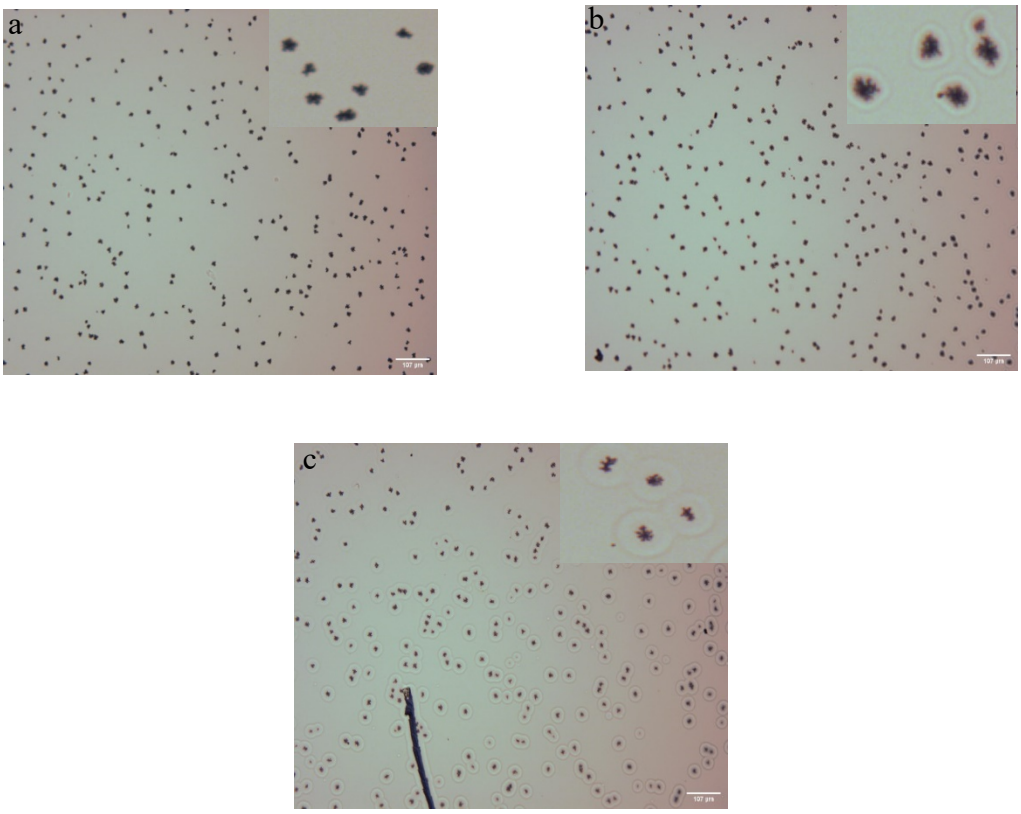

Figure 34: a) 8 hour annealed TSG b)8 hour annealed TSG submerged in ethanol solution for 15 minutes and c) 30 minutes. Here, top right corner are the zoomed images.

Also, we suggest that the thickness of native SiO2 on Silicon wafer is not enough to stop the diffusion of gold onto silicon; therefore, we tried to grow 100 nm SiO2 on Si wafer at 1000ºC using wet thermal oxidation. Before that we etched the native SiO2 from silicon wafer, and then after growing 100nm SiO2, we deposited 100 nm gold on this Si/SiO2 using e-beam evaporator (Thickness of SiO2: 100nm). This deposited gold Si wafer is annealed at 240ºC in air for 8 hours. This helped to stop the formation of Gold silicide as shown in Fig 32. After that we used this gold deposited Si wafer to make TSG. We submerged this TSG in 10% Az11 containing mSAMs for 22 hours as shown in Figure 35 b). We inferred that these bubbles were formed due to the formation of gold silicide (Figure 35 a)); however, we found that this is not the case (as shown in Figure 37). We proposed that these bubbles were formed because of these larger pinholes in TSG after we annealed the samples.

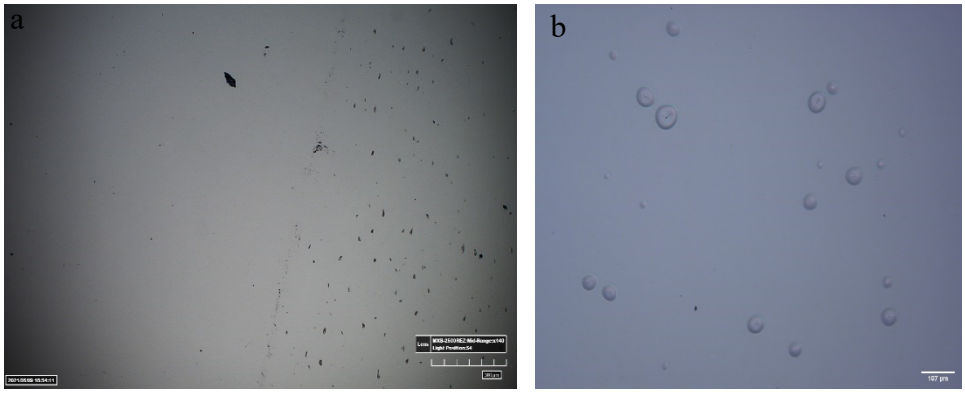

Figure 35: a) 8 hours Annealed Au deposited Si wafer at 240ºC with 100nm SiO2 sample (hirox image) and b) Submerged in 10% mSAMs for 22 hours TSG annealed for 8 hours at 240ºC with 100nm SiO2 sample.

The result was inconclusive about the formation of bubbles when we try to submerge the

unannealed TSG on Az11 containing mixed solutions for more than 1 hour. This means that it is dependent on the location from which we cleaved the TSG from the Silicon wafer. However, the result was consistent for 1 hour incubation time. Therefore, we have not submerged the unannealed TSG sample for more than 1 hour. Figure 36. shows the Scanning Electron Microscope (SEM) of the gold silicide.

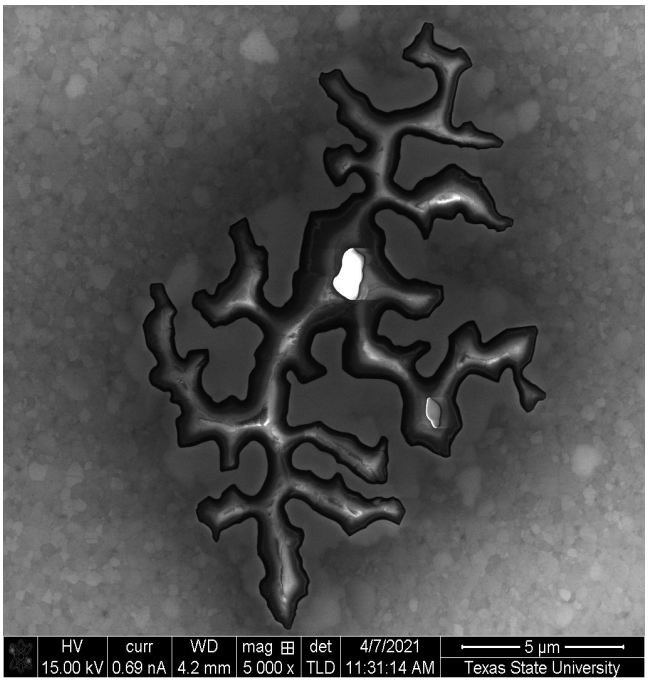

Figure 36: SEM of the gold silicide.

5.4 AFM of mixed Self-Assembled Monolayers:

In this section, we will discuss the AFM topography images of the different concentrations of mixed Self-Assembled Monolayers before UV illumination. Figure 36. shows the Tapping-Mode AFM image of 100% Az11 Self Assembled Monolayers (SAM) on TSG (2um by 2um scale). The topography image shows the 100% Az11 SAM is very closely packed. Because of this densely packed structure (steric hinderance will occur) of 100 % Az11 SAM, we did not choose this sample for the photoisomerization experiment.

We can also see the underlying gold grains in the TSG in the image.

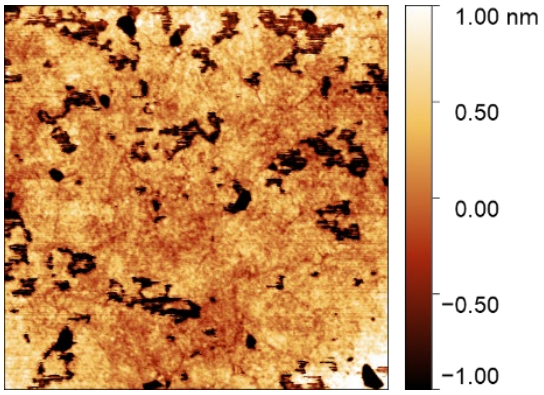

Figure 37: Tapping Mode-AFM image of 100% Az11 SAM on TSG with 2 um by 2 um scale

For the photoisomerization experiment, we chose small concentration of Az11 (typically 10% Az11 and 1% Az11). Also, we cannot see the azobenzene blobs as we can see in the smaller concentration containing Az11 SAM (Figure. 16, 39, 40) which may be because of this closely packed structure of 100% Az11 SAM.

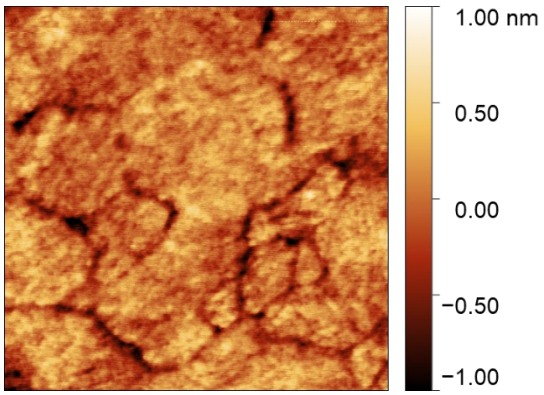

Figure 38: Tapping Mode-AFM image of 50% Az11 and 50 % C10 mixed SAMs on TSG with 0.5 um by 0.5 um scale.

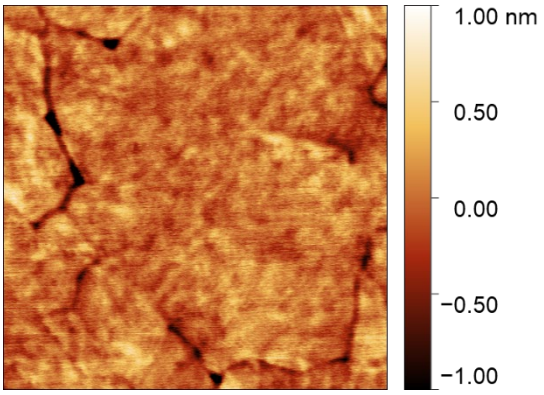

Figure 39: Tapping Mode-AFM image of 33% Az11 and 67% C10 mixed SAMs on TSG with 0.5 um by 0.5 um scale.

In 100% Az11 SAM, 50% Az11 and 50% C10 mSAMS on TSG, and 33% Az11 and 67 % C10, we cannot see the blobs as we can see in the lower concentration of Az11. We do not know if the blobs are Azobenzene yet. This will be verified by AFM imaging after the in-situ UV illumination. Figure 40. shows the Tapping-Mode AFM image of 30% Az11 containing mSAMs and from the line profile, we can see these blobs are 1 nm in height, which is expected to be the Azobenzene moieties.

Figure 41. shows the Tapping Mode- AFM image of 1% Az11 and 99% C10 mSAMs on TSG. Here, the line profile clearly shows the height of the blobs is 1nm. We suggest that these blobs may be present in the 50% sample and 33% sample, but because of the substrate defects, we could not detect these blobs. These defects may be because of the disordered structure of 30% sample and inhomogeneity. The fewer blobs shown in the 30% sample as compared to the 1% sample may be explained by the defects in TSG as it is dependent on the location of the template stripped gold from which we cleaved the gold of from Si wafer.

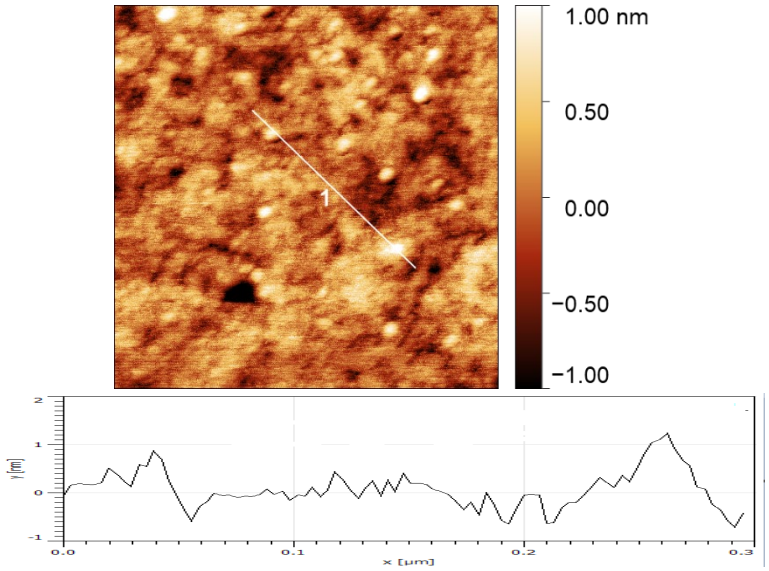

Figure 40: Tapping Mode-AFM image of 30% Az11 and 70% C10 mixed SAMs on TSG with 0.5 um by 0.5 um scale and Line profile.

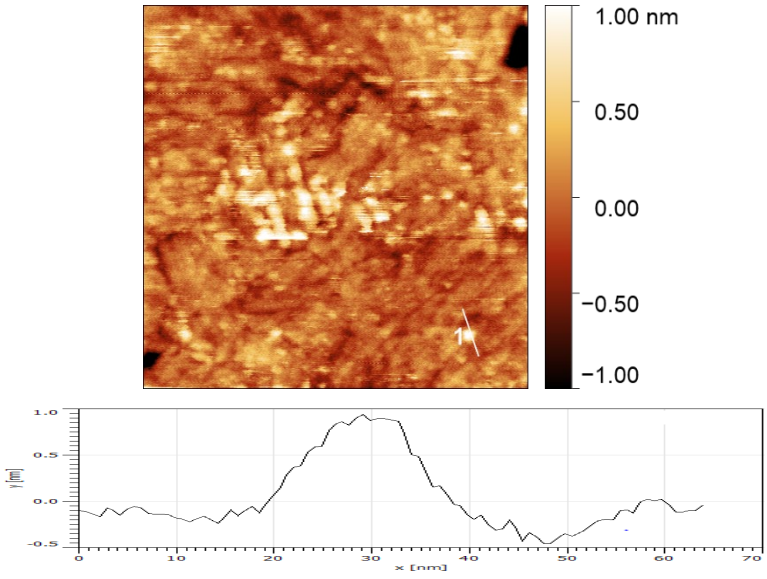

Figure 41: Tapping Mode-AFM image of 1% Az11 and 99% C10 mixed SAMs on TSG with 0.5 um by 0.5 um scale and line profile.

5.5 Kelvin Probe Atomic Force Microscopy of mixed Self-Assembled Monolayers:

The KPFM measurements were taken using JEOL AFM in our lab of mixed Self-Assembled Monolayers of 1% Az11. Fig 41. Shows the modified JEOL AFM (JSPM 5200) with Ultraviolet illumination setup. Figure 42. shows the Frequency Modulation-KPFM images of the mSAMs of 1%Az11 on TSG.

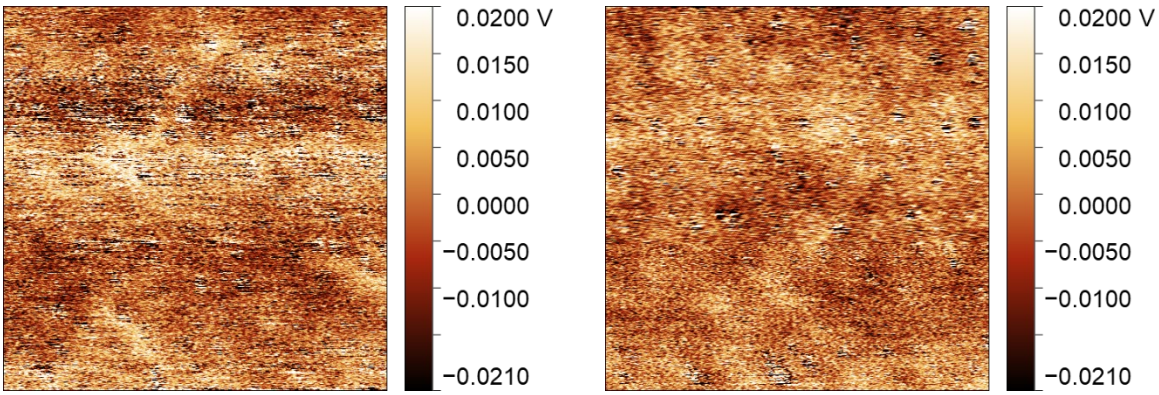

Figure 42: FM-KPFM images of mSAMs of 1%Az11 on TSG before(right) and after UV illimunation (left) (40nm by 40nm scale)

The work function of the surface of our sample is spatially resolved using the KPFM method. We see the weak contrast between these samples; therefore, we really cannot see the work function difference between the blobs and the C10 chains as we can clearly see in AFM topography images.

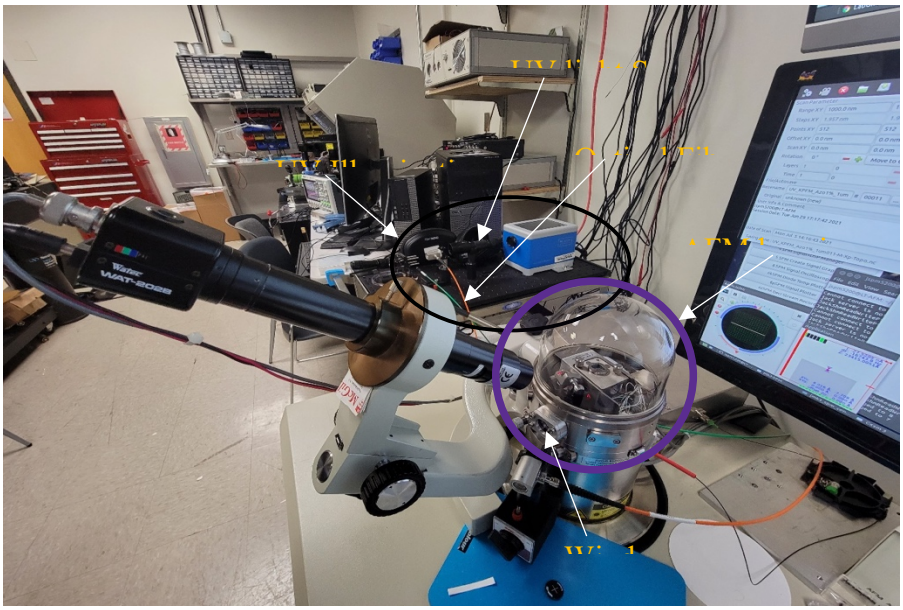

Figure 43: Modified JEOL AFM (Model JSPM-52000) with Ultraviolet illumination experiment setup.

In this UV illuminated in-situ experiment setup, the UV light coming from light source passes through the optical fiber to window. There are two mirrors (mirror tilted with 45° angle (mirror 1) and 45° angle parabolic mirror (mirror 2)) inside this AFM housing. When the UV light get into the AFM housing, this light gets reflected by mirror 1 and then again get this light is bounced by mirror 2 which eventually goes to the sample.

5.6 Photoisomerization of the Azobenzene-containing mixed Self-Assembled Monolayers on TSG:

As explained in the literature review chapter, the photoisomerization of Az11 Self-Assembled Monolayers on gold is quenched due to steric hinderance and excitonic

coupling between the monolayers; therefore, we make mixed Self-Assembled Monolayers of Az11 and C10 as a spacer for the free volume. We have used TATTU U1S UV Flashlight Rechargeable 365nm Black Light Torch, Blacklight 5W Ultraviolet (UV) LED Lamp with Micro USB Charging Cable (as shown in Figure. 44) for Ultraviolet illumination. The UV illumination was performed in-situ. We have used modified JEOL AFM with UV illumination experimental setup (Fig. 43). The incubation time for this 1% Az11 mSAMs is one hour. Figure 45. shows the Frequency-Modulation AFM topography images in vacuum with the modified JEOL AFM (JSPM-5200) of mixed SAMs of 1% AZ11 before and after the Ultraviolet illumination for 7 minutes.

Figure 44: UV illumination Flashlight (wavelength= 365nm)

The distinction between these images is shown clearly by black rectangular region with arrows inside in this region. Especially, the blobs pointed by arrows (black, blue, and yellow) are absent after UV illumination. This means there is likely that the trans-state of Azobenzene on mSAMs upon UV illumination changes to cis state. Here, if we take black rectangular region as shown in topography images, these blobs which we expected to azobenzene were diminished after we illuminate with UV light. We suggest these blobs changes its conformation from trans-state to cis state. We do not see changes in other blobs because it is dependent upon where we illuminate the UV light.

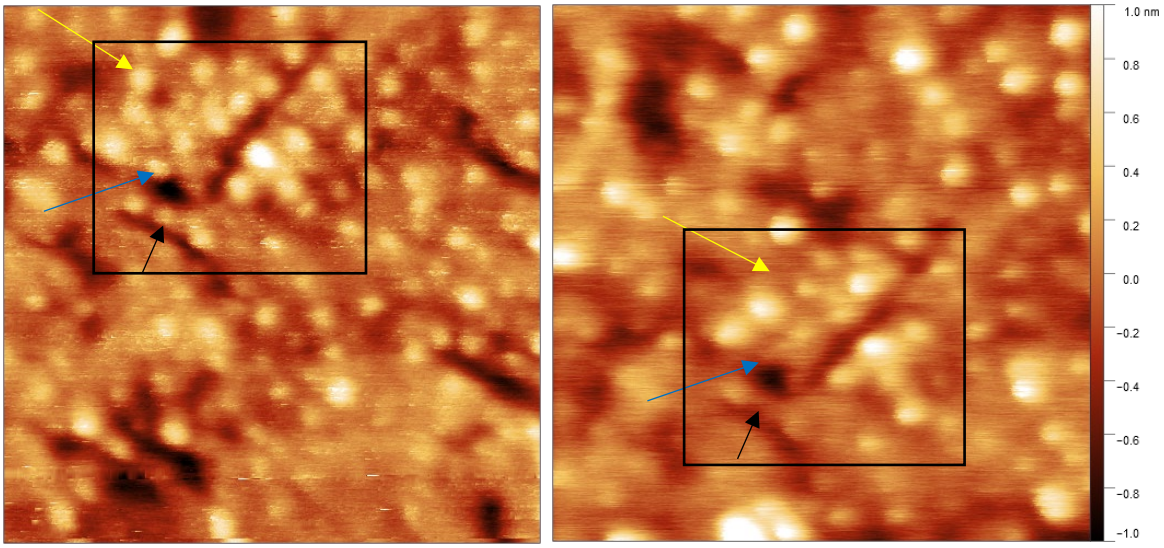

Figure 45: AFM topography images of 1%Az11 mSAMs before (left) and after Ultraviolet illumination in vacuum (right) (Scan sizes are 250 *250 nm). Arrows showing the changes before and after UV illumination.

6. CONCLUSIONS AND OUTLOOK

In this chapter, we summarized all the results when we characterize our samples. Also, we explain about the considerations for the future work.

Conclusions:

In this chapter, we summarize our results on four different experiments:

1) Preparation of Template Stripped Gold on Si/SiO2

2) Preparation of the mixed self-assembled of Az11 and C10 on top of this Template Stripped Gold on Si/SiO2.

3) FTIR and Tapping Mode- AFM topography images of Azobenzene-functionalized mSAMs on TSG.

4) Photoisomerization of the Azobenzene-functionalized mSAMs on TSG using FM-Atomic Force Microscopy Topography images.

1) The important part of making the self-assembled monolayers is the need for a flatness of gold surface. We tried several protocols for the preparation of the ultra-flat template stripped gold. We tried is to etch the native SiO2 from the Si wafer using Buffered etched oxide in order to get the flat silicon wafer. However, from our experiment we conclude that we need SiO2 to cleave the template stripped gold from Si wafer because the bonding between Si-Au is strong. Second, we evaporated gold on Si/SiO2 and then we place small silicon coupons with epoxy glue on top of the Si/SiO2/Au making sandwich structure of (wafer)Si/SiO2/Au/epoxy/Si(coupons) (as shown in Figure. 9). After cleaving the gold, we get the unannealed template stripped gold. Thirdly, we annealed e-beam evaporated gold

on Si/SiO2 for one hour at 300 ℃ and rest of the process is the same as we explain in the second method. We compare mean square roughness of unannealed template stripped gold (R_s = 682.1 pm).to annealed template stripped gold. We conclude that the roughness of the annealed TSG is lower than the unannealed TSG (R_s = 301.7 pm).

2)The method for the preparation of mSAMs on TSG is explained in the sample preparation chapter. We used annealed TSG as a substrate for mSAMs. Nevertheless, we found that the defects in annealed TSG likely due to the gold silicide formation to form bubbles even after 15 minutes incubation in mixed Az11 and C10 solutions. Therefore, we used unannealed TSG for the preparation of mSAMs. We tried different concentrations (1%, 10%, 30%, 33%, and 50%) of Az11 to prepare mSAMs. The incubation time for all is 1 hour. We chose this incubation time because these defects due to gold silicide formation present even in the unannealed TSG. It is dependent on location of Si/SiO2/Au wafer from which we cleave the gold from. However, we found that consistent results in the absence of bubbles when we incubated the unannealed TSG for 1 hour in mixed solutions of Az11 and C10.

3) After the preparation of the mSAMs on unannealed TSG, we characterized this sample with FTIR and AFM. We conclude that from FTIR results, azobenzene is present because we found the peaks corresponding to azobenzene on mSAMs. The topography images of different concentrations (1%, 10%, 30%, 33%, and 50%) of Az11 is shown in the results section. Due to the defects present in the unannealed TSG and the densely packed azobenzene moieties in mSAMs of higher concentrations greater than 30% Az11, we could not see the blobs which we expected to be azobenzene moieties. We can clearly see the blobs likely to be azobenzene moieties in the 30%, 10 %, and 1% Az11 containing mSAMs.

The smaller presence of the blobs in 30% and 10% sample than in 1% sample is rather counterintuitive. We conclude that the fewer blobs shown in the 30% sample as compared to the 1% sample may be explained by the defects in TSG as it is dependent on the location of the template stripped gold from which we cleaved the gold of from Si wafer.

4) We chose small concentration of Az11 for the photoisomerization of azobenzene molecules. Here, we use 1% of Az11 containing mSAMs sample. We can see the blobs present in AFM topography images which is 1nm in height and 20 nm wide expected to be azobenzene moieties. After the Ultraviolet light illumination with wavelength of 365 nm, we see these blobs are decreased in height. Some of these blobs are even absent after photoisomerization. This decrease in height of these blobs and absent of some blobs likely be due to the location of UV illumination. We see these number of blobs are decreased if we take a whole region of AFM topography images. From this result we can conclude that these blobs are photoinduced, however we are likely to confirm that these blobs belong to azobenzene molecules.

Outlooks:

In this section, we discuss the probable future work that can be done further in this work. Our goal is to do Electric-Field Isomerization of this Azobenzene-functionalized mixed Self-Assembled Monolayers from the start; however, we could not get results to show it. This can be considered as a future work. It will be interesting to explore more about these blobs with Photoinduced Force Microscopy (PiFM) so that we can confirm these blobs are the azobenzene [122], [123].

RFERENCES

[1] H. H. Radamson *et al.*, “Miniaturization of CMOS,” *Micromachines*, vol. 10, no. 5, p. 293, Apr. 2019, doi: 10.3390/mi10050293.

[2] T. Tamaki and T. Ogawa, “Nonlinear and Nonsymmetric Single-Molecule Electronic Properties Towards Molecular Information Processing,” *Top. Curr. Chem.*, vol. 375, no. 5, p. 79, Oct. 2017, doi: 10.1007/s41061-017-0167-y.

[3] J. M. Abendroth, O. S. Bushuyev, P. S. Weiss, and C. J. Barrett, “Controlling Motion at the Nanoscale: Rise of the Molecular Machines,” *ACS Nano*, vol. 9, no. 8, pp. 7746–7768, Aug. 2015, doi: 10.1021/acsnano.5b03367.

[4] L. Grill, “Functionalized molecules studied by STM: motion, switching and reactivity,” *J. Phys. Condens. Matter*, vol. 20, no. 5, p. 053001, Feb. 2008, doi: 10.1088/0953-8984/20/05/053001.

[5] J. García-Amorós and D. Velasco, “Recent advances towards azobenzene-based light-driven real-time information-transmitting materials,” *Beilstein J. Org. Chem.*, vol. 8, pp. 1003–1017, Jul. 2012, doi: 10.3762/bjoc.8.113.

[6] R. Klajn, “Immobilized azobenzenes for the construction of photoresponsive materials,” *Pure Appl. Chem.*, vol. 82, no. 12, pp. 2247–2276, 2010, doi: 10.1351/PAC-CON-10-09-04.

[7] F. Schreiber, “Structure and growth of self-assembling monolayers,” *Prog. Surf. Sci.*, vol. 65, no. 5–8, pp. 151–257, 2000, doi: 10.1016/S0079-6816(00)00024-1.

[8] J. Griffiths, “II. Photochemistry of azobenzene and its derivatives,” *Chem. Soc. Rev.*, vol. 1, no. 4, p. 481, 1972, doi: 10.1039/cs9720100481.

[9] G. S. Kumar and D. C. Neckers, “Photochemistry of azobenzene-containing polymers,” *Chem. Rev.*, vol. 89, no. 8, pp. 1915–1925, Dec. 1989, doi: 10.1021/cr00098a012.

[10] A. G. Griesbeck, “Essentials of Molecular Photochemistry. VonA. Gilbert undJ. Baggott. Blackwell Scientific Publications, Oxford 1991. XII, 538 S. kartoniert £ 17.95. - ISBN 0-632-02429-1,” *Angew. Chemie*, vol. 103, no. 11, pp. 1554–1555, Nov. 1991, doi: 10.1002/ange.19911031143.

[11] C. R. Crecca and A. E. Roitberg, “Theoretical Study of the Isomerization Mechanism of Azobenzene and Disubstituted Azobenzene Derivatives,” *J. Phys. Chem. A*, vol. 110, no. 26, pp. 8188–8203, Jul. 2006, doi: 10.1021/jp057413c.

[12] H. Akiyama, K. Tamada, J. Nagasawa, K. Abe, and T. Tamaki, “Photoreactivity in self-assembled monolayers formed from asymmetric disulfides having para-substituted azobenzenes,” *J. Phys. Chem. B*, 2003, doi: 10.1021/jp026103g.

[13] H.-J. Timpe, “Photochromism - molecules and systems. Herausgeber: Dürr, H., Bouas-Laurent, H. 1. Auflage, 1068 S. Amsterdam, Oxford, New York, Tokyo: Elsevier, 1990. Schriftenreihe: Studies in organic chemistry, 40. ISBN 0-444-87432-1,” *J. für Prakt. Chemie*, vol. 333, no. 5, pp. 811–812, 1991, doi: 10.1002/prac.19913330522.

[14] T. Moldt, “Photoswitching Kinetics of Azobenzene-Alkanethiols on Gold (111),” no. 111, 2019.

[15] A. Cembran, F. Bernardi, M. Garavelli, L. Gagliardi, and G. Orlandi, “On the Mechanism of the cis−trans Isomerization in the Lowest Electronic States of Azobenzene: S 0 , S 1 , and T 1,” *J. Am. Chem. Soc.*, vol. 126, no. 10, pp. 3234–3243, Mar. 2004, doi: 10.1021/ja038327y.

[16] N. Tamai and H. Miyasaka, “Ultrafast Dynamics of Photochromic Systems,” *Chem. Rev.*, vol. 100, no. 5, pp. 1875–1890, May 2000, doi: 10.1021/cr9800816.

[17] I. K. Lednev, T.-Q. Ye, R. E. Hester, and J. N. Moore, “Femtosecond Time-Resolved UV−Visible Absorption Spectroscopy of trans -Azobenzene in Solution,” *J. Phys. Chem.*, vol. 100, no. 32, pp. 13338–13341, Jan. 1996, doi: 10.1021/jp9610067.

[18] T. Nägele, R. Hoche, W. Zinth, and J. Wachtveitl, “Femtosecond photoisomerization of cis-azobenzene,” *Chem. Phys. Lett.*, vol. 272, no. 5–6, pp. 489–495, Jul. 1997, doi: 10.1016/S0009-2614(97)00531-9.

[19] H. Satzger, S. Spörlein, C. Root, J. Wachtveitl, W. Zinth, and P. Gilch, “Fluorescence spectra of trans- and cis-azobenzene – emission from the Franck–Condon state,” *Chem. Phys. Lett.*, vol. 372, no. 1–2, pp. 216–223, Apr. 2003, doi: 10.1016/S0009-2614(03)00364-6.

[20] M. Alemani, M. V. Peters, S. Hecht, K. H. Rieder, F. Moresco, and L. Grill, “Electric field-induced isomerization of azobenzene by STM,” *J. Am. Chem. Soc.*, 2006, doi: 10.1021/ja065449s.

[21] M. J. Comstock *et al.*, “Reversible Photomechanical Switching of Individual Engineered Molecules at a Metallic Surface,” *Phys. Rev. Lett.*, vol. 99, no. 3, p. 038301, Jul. 2007, doi: 10.1103/PhysRevLett.99.038301.

[22] R. J. Maurer and K. Reuter, “Computational design of metal-supported molecular switches: transient ion formation during light- and electron-induced isomerisation of azobenzene,” *J. Phys. Condens. Matter*, vol. 31, no. 4, p. 044003, Jan. 2019, doi: 10.1088/1361-648X/aaf0e1.

[23] S. Hagen, P. Kate, M. V. Peters, S. Hecht, M. Wolf, and P. Tegeder, “Kinetic analysis of the photochemically and thermally induced isomerization of an azobenzene derivative on Au(111) probed by two-photon photoemission,” *Appl. Phys. A*, vol. 93, no. 2, pp. 253–260, Nov. 2008, doi: 10.1007/s00339-008-4831-5.

[24] A. Ulman, “Formation and Structure of Self-Assembled Monolayers,” *Chem. Rev.*, vol. 96, no. 4, pp. 1533–1554, Jan. 1996, doi: 10.1021/cr9502357.

[25] C. Vericat, M. E. Vela, G. Benitez, P. Carro, and R. C. Salvarezza, “Self-assembled monolayers of thiols and dithiols on gold: new challenges for a well-known system,” *Chem. Soc. Rev.*, vol. 39, no. 5, p. 1805, 2010, doi: 10.1039/b907301a.

[26] R. Klajn, “Immobilized azobenzenes for the construction of photoresponsive materials,” *Pure Appl. Chem.*, vol. 82, no. 12, pp. 2247–2279, Oct. 2010, doi: 10.1351/PAC-CON-10-09-04.

[27] C. Gahl *et al.*, “Structure and Excitonic Coupling in Self-Assembled Monolayers of Azobenzene-Functionalized Alkanethiols,” *J. Am. Chem. Soc.*, vol. 132, no. 6, pp. 1831–1838, Feb. 2010, doi: 10.1021/ja903636q.

[28] N. Heinemann *et al.*, “Reversible switching in self-assembled monolayers of azobenzene thiolates on Au (111) probed by threshold photoemission,” *Chem. Phys.*, vol. 402, pp. 22–28, Jun. 2012, doi: 10.1016/j.chemphys.2012.03.025.

[29] T. Nagahiro, H. Akiyama, M. Hara, and K. Tamada, “Photoisomerization of azobenzene containing self-assembled monolayers investigated by Kelvin probe work function measurements,” *J. Electron Spectros. Relat. Phenomena*, vol. 172, no. 1–3, pp. 128–133, May 2009, doi: 10.1016/j.elspec.2009.02.009.

[30] B. Stiller *et al.*, “Optically Induced Switching of Azobenzene Containing Self Assembling Monolayers Investigated by Kelvin Probe and Scanning Force Microscopy,” *Mol. Cryst. Liq. Cryst. Sci. Technol. Sect. A. Mol. Cryst. Liq. Cryst.*, vol. 355, no. 1, pp. 401–411, Jan. 2001, doi: 10.1080/10587250108023673.

[31] U. Jung *et al.*, “Photoswitching Behavior of Azobenzene-Containing Alkanethiol Self-Assembled Monolayers on Au Surfaces,” *Langmuir*, vol. 26, no. 17, pp. 13913–13923, Sep. 2010, doi: 10.1021/la1015109.

[32] D. T. Valley, M. Onstott, S. Malyk, and A. V. Benderskii, “Steric Hindrance of Photoswitching in Self-Assembled Monolayers of Azobenzene and Alkane Thiols,” *Langmuir*, vol. 29, no. 37, pp. 11623–11631, Sep. 2013, doi: 10.1021/la402144g.

[33] 2021 from https://pubchem.ncbi.nlm.nih.gov/compound/1-Decanethiol. National Center for Biotechnology Information (2021). PubChem Compound Summary for CID 8917, 1-Decanethiol. Retrieved May 21, “No Title.”

[34] J. Wen, Z. Tian, and J. Ma, “Light- and electric-field-induced switching of thiolated azobenzene self-assembled monolayer,” *J. Phys. Chem. C*, vol. 117, no. 39, pp. 19934–19944, 2013, doi: 10.1021/jp404434r.

[35] L. Q. Zheng, X. Wang, F. Shao, M. Hegner, and R. Zenobi, “Nanoscale Chemical Imaging of Reversible Photoisomerization of an Azobenzene-Thiol Self-Assembled Monolayer by Tip-Enhanced Raman Spectroscopy,” *Angew. Chemie - Int. Ed.*, vol. 57, no. 4, pp. 1025–1029, 2018, doi: 10.1002/anie.201710443.

[36] M. Alemani, “Low Temperature STM Investigation of Molecular Manipulation, Decoupling and Switching,” 2007.

[37] N. Biswas and S. Umapathy, “Density Functional Calculations of Structures, Vibrational Frequencies, and Normal Modes of trans - and cis -Azobenzene,” *J. Phys. Chem. A*, vol. 101, no. 30, pp. 5555–5566, Jul. 1997, doi: 10.1021/jp970312x.

[38] N. Kurita, T. Ikegami, and Y. Ishikawa, “Ab initio study of the minimum-energy structure of trans-azobenzene,” *Chem. Phys. Lett.*, vol. 360, no. 3–4, pp. 349–354, Jul. 2002, doi: 10.1016/S0009-2614(02)00854-0.

[39] E. R. Talaty and J. C. Fargo, “Thermal cis–trans-isomerization of substituted azobenzenes: a correction of the literature,” *Chem. Commun. (London)*, no. 2, pp. 65–66, 1967, doi: 10.1039/C19670000065.

[40] P. Cattaneo and M. Persico, “An ab initio study of the photochemistry of azobenzene,” *Phys. Chem. Chem. Phys.*, vol. 1, no. 20, pp. 4739–4743, 1999, doi: 10.1039/a905055h.

[41] M. L. Tiago, S. Ismail-Beigi, and S. G. Louie, “Photoisomerization of azobenzene from first-principles constrained density-functional calculations,” *J. Chem. Phys.*, vol. 122, no. 9, p. 094311, Mar. 2005, doi: 10.1063/1.1861873.

[42] P. Hamm, S. M. Ohline, and W. Zinth, “Vibrational cooling after ultrafast photoisomerization of azobenzene measured by femtosecond infrared spectroscopy,” *J. Chem. Phys.*, vol. 106, no. 2, pp. 519–529, Jan. 1997, doi: 10.1063/1.473392.

[43] T. Ishikawa, T. Noro, and T. Shoda, “Theoretical study on the photoisomerization of azobenzene,” *J. Chem. Phys.*, vol. 115, no. 16, pp. 7503–7512, Oct. 2001, doi: 10.1063/1.1406975.

[44] B. K. Pathem, S. A. Claridge, Y. B. Zheng, and P. S. Weiss, “Molecular Switches and Motors on Surfaces,” *Annu. Rev. Phys. Chem.*, vol. 64, no. 1, pp. 605–630, Apr. 2013, doi: 10.1146/annurev-physchem-040412-110045.

[45] J. C. Love, L. A. Estroff, J. K. Kriebel, R. G. Nuzzo, and G. M. Whitesides, “Self-Assembled Monolayers of Thiolates on Metals as a Form of Nanotechnology,” *Chem. Rev.*, vol. 105, no. 4, pp. 1103–1170, Apr. 2005, doi: 10.1021/cr0300789.

[46] L. H. Dubois and R. G. Nuzzo, “Synthesis, Structure, and Properties of Model Organic Surfaces,” *Annu. Rev. Phys. Chem.*, vol. 43, no. 1, pp. 437–463, Oct. 1992, doi: 10.1146/annurev.pc.43.100192.002253.

[47] C. D. Bain, E. B. Troughton, Y. T. Tao, J. Evall, G. M. Whitesides, and R. G. Nuzzo, “Formation of monolayer films by the spontaneous assembly of organic thiols from solution onto gold,” *J. Am. Chem. Soc.*, vol. 111, no. 1, pp. 321–335, Jan. 1989, doi: 10.1021/ja00183a049.

[48] J. Sagiv, “Organized monolayers by adsorption. 1. Formation and structure of oleophobic mixed monolayers on solid surfaces,” *J. Am. Chem. Soc.*, vol. 102, no. 1, pp. 92–98, Jan. 1980, doi: 10.1021/ja00521a016.

[49] D. Witt, R. Klajn, P. Barski, and B. Grzybowski, “Applications, Properties and Synthesis of ω-Functionalized n-Alkanethiols and Disulfides - the Building Blocks of Self-Assembled Monolayers,” *Curr. Org. Chem.*, vol. 8, no. 18, pp. 1763–1797, Dec. 2004, doi: 10.2174/1385272043369421.

[50] P. Dietrich *et al.*, “An anchoring strategy for photoswitchable biosensor technology: azobenzene-modified SAMs on Si(111),” *Appl. Phys. A*, vol. 93, no. 2, pp. 285–292, Nov. 2008, doi: 10.1007/s00339-008-4828-0.

[51] M. Min, G. S. Bang, H. Lee, and B.-C. Yu, “A photoswitchable methylene-spaced fluorinated aryl azobenzene monolayer grafted on silicon,” *Chem. Commun.*, vol. 46, no. 29, p. 5232, 2010, doi: 10.1039/c0cc00521e.

[52] L. M. Siewierski, W. J. Brittain, S. Petrash, and M. D. Foster, “Photoresponsive Monolayers Containing In-Chain Azobenzene,” *Langmuir*, vol. 12, no. 24, pp. 5838–5844, Jan. 1996, doi: 10.1021/la960506o.

[53] F. Hamelmann *et al.*, “Thin molybdenum oxide films produced by molybdenum pentacarbonyl 1-methylbutylisonitrile with plasma-assisted chemical vapor deposition,” *Thin Solid Films*, vol. 446, no. 2, pp. 167–171, Jan. 2004, doi: 10.1016/j.tsf.2003.09.045.

[54] J. G. Victor and J. M. Torkelson, “On measuring the distribution of local free volume in glassy polymers by photochromic and fluorescence techniques,” *Macromolecules*, vol. 20, no. 9, pp. 2241–2250, Sep. 1987, doi: 10.1021/ma00175a032.

[55] W. B. Caldwell *et al.*, "A Highly Ordered Self-Assembled Monolayer Film of an Azobenzenealkanethiol on Au(111): Electrochemical Properties and Structural Characterization by Synchrotron in-Plane X-ray Diffraction, Atomic Force Microscopy, and Surface-Enhanced Raman Spectroscopy," *J. Am. Chem. Soc.*, vol. 117, no. 22, pp. 6071–6082, Jun. 1995, doi: 10.1021/ja00127a021.

[56] R. Wang, T. Iyoda, L. Jiang, D. A. Tryk, K. Hashimoto, and A. Fujishima, "Structural investigation of azobenzene-containing self-assembled monolayer films," *J. Electroanal. Chem.*, vol. 438, no. 1–2, pp. 213–219, Nov. 1997, doi: 10.1016/S0022-0728(96)05031-0.

[57] H. Wolf *et al.*, "End-group-dominated molecular order in self-assembled monolayers," *J. Phys. Chem.*, vol. 99, no. 18, pp. 7102–7107, 1995, doi: 10.1021/j100018a050.

[58] E. Delamarche, B. Michel, H. Kang, and C. Gerber, "Thermal Stability of Self-Assembled Monolayers," *Langmuir*, vol. 10, no. 11, pp. 4103–4108, Nov. 1994, doi: 10.1021/la00023a033.

[59] M. Jaschke *et al.*, "Structure of Alkyl and Perfluoroalkyl Disulfide and Azobenzenethiol Monolayers on Gold(111) Revealed by Atomic Force Microscopy," *J. Phys. Chem.*, vol. 100, no. 6, pp. 2290–2301, Jan. 1996, doi: 10.1021/jp952355o.

[60] R. Wang, T. Iyoda, L. Jiang, K. Hashimoto, and A. Fujishima, "Molecular Arrangement in an Azobenzene-Terminated Self-Assembled Monolayer Film," *Chem. Lett.*, vol. 25, no. 11, pp. 1005–1006, Nov. 1996, doi: 10.1246/cl.1996.1005.

[61] K. Tamada *et al.*, “Structure and Growth of Hexyl Azobenzene Thiol SAMs on Au(111),” *Langmuir*, vol. 14, no. 12, pp. 3264–3271, Jun. 1998, doi: 10.1021/la971348j.

[62] K. Tamada *et al.*, “Structure of SAMs generated from functionalized thiols on gold,” *Thin Solid Films*, vol. 327–329, pp. 150–155, Aug. 1998, doi: 10.1016/S0040-6090(98)00618-X.

[63] “This conclusion is in agreement with experiments on electrostatically stabilized mixed mono-layers of AB [55], which show that the photoisomerization is hampered when the surface area per AB group is smaller that 0.45 nm2.”

[64] M. Nakagawa, R. Watase, and K. Ichimura, “Preparation of Monolayers of Ion-Paired Macrocyclic Amphiphiles to Estimate a Critical Free Space Required for Azobenzene Photoisomerization,” *Chem. Lett.*, vol. 28, no. 11, pp. 1209–1210, Nov. 1999, doi: 10.1246/cl.1999.1209.

[65] E. Titov, G. Granucci, J. P. Götze, M. Persico, and P. Saalfrank, “Dynamics of Azobenzene Dimer Photoisomerization: Electronic and Steric Effects,” *J. Phys. Chem. Lett.*, vol. 7, no. 18, pp. 3591–3596, Sep. 2016, doi: 10.1021/acs.jpclett.6b01401.

[66] U. Jung *et al.*, “Structure and redox behavior of azobenzene-containing monolayers on Au(111): A combined STM, X-ray reflectivity, and voltammetry study,” *J. Electroanal. Chem.*, vol. 619–620, pp. 152–158, Jul. 2008, doi: 10.1016/j.jelechem.2008.04.002.

[67] T. Kondo, T. Kanai, and K. Uosaki, “Control of the Charge-Transfer Rate at a Gold Electrode Modified with a Self-Assembled Monolayer Containing Ferrocene and Azobenzene by Electro- and Photochemical Structural Conversion of Cis and Trans Forms of the Azobenzene Moiety,” *Langmuir*, vol. 17, no. 20, pp. 6317–6324, Oct. 2001, doi: 10.1021/la0108914.

[68] H.-Z. Yu *et al.*, “Fabricating electroactive azobenzene self-assembled monolayers and their characterization,” *J. Electroanal. Chem.*, vol. 395, no. 1–2, pp. 327–330, Oct. 1995, doi: 10.1016/0022-0728(95)04230-L.

[69] H.-Z. Yu *et al.*, “Electrochemical Behavior of Azobenzene Self-Assembled Monolayers on Gold,” *Langmuir*, vol. 12, no. 11, pp. 2843–2848, Jan. 1996, doi: 10.1021/la950632c.

[70] S. Karpe *et al.*, “Oligothiophene-derivatized azobenzene as immobilized photoswitchable conjugated systems,” *Chem. Commun.*, vol. 46, no. 21, p. 3657, 2010, doi: 10.1039/c002072a.

[71] H. Akiyama, K. Tamada, J. Nagasawa, K. Abe, and T. Tamaki, “Photoreactivity in Self-Assembled Monolayers Formed from Asymmetric Disulfides Having para-Substituted Azobenzenes,” *J. Phys. Chem. B*, vol. 107, no. 1, pp. 130–135, Jan. 2003, doi: 10.1021/jp026103g.

[72] M. Han, D. Ishikawa, T. Honda, E. Ito, and M. Hara, “Light-driven molecular switches in azobenzene self-assembled monolayers: effect of molecular structure on reversible photoisomerization and stable cis state,” *Chem. Commun.*, vol. 46, no. 20, p. 3598, 2010, doi: 10.1039/b921801g.

[73] I. Willner, V. Pardo-Yissar, E. Katz, and K. T. Ranjit, “A photoactivated ‘molecular train’ for optoelectronic applications: light-stimulated translocation of a β-cyclodextrin receptor within a stoppered azobenzene-alkyl chain supramolecular monolayer assembly on a Au-electrode,” *J. Electroanal. Chem.*, vol. 497, no. 1–2, pp. 172–177, Feb. 2001, doi: 10.1016/S0022-0728(00)00455-1.

[74] D. Ishikawa, T. Honda, E. Ito, M. Han, and M. Hara, “Photoisomerization of Sterically Hindered Azobenzenes in Self-Assembled Monolayers on Gold Surfaces,” *Jpn. J. Appl. Phys.*, vol. 49, no. 6, p. 06GH12, Jun. 2010, doi: 10.1143/JJAP.49.06GH12.

[75] C. Li, B. Ren, Y. Zhang, Z. Cheng, X. Liu, and Z. Tong, “A Novel Ferroceneylazobenzene Self-Assembled Monolayer on an ITO Electrode: Photochemical and Electrochemical Behaviors,” *Langmuir*, vol. 24, no. 22, pp. 12911–12918, Nov. 2008, doi: 10.1021/la802101g.

[76] S. W. Han, C. H. Kim, S. H. Hong, Y. K. Chung, and K. Kim, “Azobenzene-Incorporated Alkanethiol Monolayer Film on Au(111): Reflection-Absorption Infrared Spectroscopy and Atomic Force Microscopy Study,” *Langmuir*, vol. 15, no. 4, pp. 1579–1583, 1999, doi: 10.1021/la9807457.

[77] B. Stiller *et al.*, “Optically induced switching of azobenzene containing self assembling monolayers investigated by Kelvin probe and scanning force microscopy,” *Mol. Cryst. Liq. Cryst. Sci. Technol. Sect. A Mol. Cryst. Liq. Cryst.*, vol. 355, pp. 401–411, 2001, doi: 10.1080/10587250108023673.

[78] S. C. B. Mannsfeld *et al.*, "The structure of [4-(phenylazo)phenoxy]hexane-1-thiol self-assembled monolayers on Au(111)," *J. Phys. Chem. B*, vol. 106, no. 9, pp. 2255–2260, 2002, doi: 10.1021/jp012771a.

[79] A. S. Kumar *et al.*, "Reversible photo-switching of single azobenzene molecules in controlled nanoscale environments," *Nano Lett.*, vol. 8, no. 6, pp. 1644–1648, 2008, doi: 10.1021/nl080323+.

[80] U. Jung *et al.*, "Photoswitching behavior of azobenzene-containing alkanethiol self-assembled monolayers on Au surfaces," *Langmuir*, vol. 26, no. 17, pp. 13913–13923, 2010, doi: 10.1021/la1015109.

[81] M. Kaneta, T. Honda, K. Onda, and M. Han, "Repeated photoswitching performance of azobenzenes adsorbed on gold surfaces: a balance between space, intermolecular interactions, and phase separation," *New J. Chem.*, vol. 41, no. 4, pp. 1827–1833, 2017, doi: 10.1039/c6nj03121h.

[82] M. J. Cook, A.-M. Nygård, Z. Wang, and D. A. Russell, "An evanescent field driven mono-molecular layer photoswitch: coordination and release of metallated macrocycles," *Chem. Commun.*, no. 10, pp. 1056–1057, May 2002, doi: 10.1039/b201870p.

[83] Y. B. Zheng *et al.*, "Surface-Enhanced Raman Spectroscopy to Probe Reversibly Photoswitchable Azobenzene in Controlled Nanoscale Environments," *Nano Lett.*, vol. 11, no. 8, pp. 3447–3452, Aug. 2011, doi: 10.1021/nl2019195.

[84] S. Imabayashi, N. Gon, T. Sasaki, D. Hobara, and T. Kakiuchi, “Effect of Nanometer-Scale Phase Separation on Wetting of Binary Self-Assembled Thiol Monolayers on Au(111),” *Langmuir*, vol. 14, no. 9, pp. 2348–2351, Apr. 1998, doi: 10.1021/la971377u.

[85] G. Pace, A. Petitjean, M.-N. Lalloz-Vogel, J. Harrowfield, J.-M. Lehn, and P. Samorì, “Subnanometer-Resolved Patterning of Bicomponent Self-Assembled Monolayers on Au(111),” *Angew. Chemie Int. Ed.*, vol. 47, no. 13, pp. 2484–2488, Mar. 2008, doi: 10.1002/anie.200704731.

[86] S. Chen, L. Li, C. L. Boozer, and S. Jiang, “Controlled Chemical and Structural Properties of Mixed Self-Assembled Monolayers by Coadsorption of Symmetric and Asymmetric Disulfides on Au(111),” *J. Phys. Chem. B*, vol. 105, no. 15, pp. 2975–2980, Apr. 2001, doi: 10.1021/jp0040650.

[87] T. Moldt *et al.*, “Tailoring the Properties of Surface-Immobilized Azobenzenes by Monolayer Dilution and Surface Curvature,” *Langmuir*, vol. 31, no. 3, pp. 1048–1057, Jan. 2015, doi: 10.1021/la504291n.

[88] S. Watcharinyanon, *Structure of Self-Assembled Monolayers on Gold Studied by NEXAFS and Photoelectron Spectroscopy*. 2008.

[89] N. Vogel, J. Zieleniecki, and I. Köper, “As flat as it gets: Ultrasmooth surfaces from template-stripping procedures,” *Nanoscale*, vol. 4, no. 13, pp. 3820–3832, 2012, doi: 10.1039/c2nr30434a.

[90] P. Wagner, M. Hegner, H.-J. Giintherodt, and G. Semenza, “Formation and in Situ Modification of Monolayers Chemisorbed on Ultraflat Template-Stripped Gold Surfaces,” 1995. [Online]. Available: https://pubs.acs.org/sharingguidelines.

[91] P. Wagner, F. Zaugg, P. Kernen, M. Hegner, and G. Semenza, “functionalized self-assembled monolayers chemisorbed on ultraflat Au(111) surfaces for biological scanning probe microscopy in aqueous buffers,” 1996.

[92] E. A. Weiss, G. K. Kaufman, J. K. Kriebel, Z. Li, R. Schalek, and G. M. Whitesides, “Si/SiO2-templated formation of ultraflat metal surfaces on glass, polymer, and solder supports: Their use as substrates for self-assembled monolayers,” *Langmuir*, vol. 23, no. 19, pp. 9686–9694, Sep. 2007, doi: 10.1021/la701919r.

[93] M. Lastapis, “Picometer-Scale Electronic Control of Molecular Dynamics Inside a Single Molecule,” *Science (80-.).*, vol. 308, no. 5724, pp. 1000–1003, May 2005, doi: 10.1126/science.1108048.

[94] G. Füchsel, T. Klamroth, J. Dokić, and P. Saalfrank, “On the Electronic Structure of Neutral and Ionic Azobenzenes and Their Possible Role as Surface Mounted Molecular Switches,” *J. Phys. Chem. B*, vol. 110, no. 33, pp. 16337–16345, Aug. 2006, doi: 10.1021/jp060969v.

[95] P. Saalfrank, “Manipulation of adsorbates with electric fields,” *J. Chem. Phys.*, vol. 113, no. 9, pp. 3780–3791, 2000, doi: 10.1063/1.1287656.

[96] H. Ibach , Harald, Lüth, *Festkörperphysik*. 2008.

[97] A. Davydov, *Theory of Molecular Excitons*. Plenum Press, New York - London, 1971, 1971.

[98] E. R. Events, “Harrisonn Robert Gri n Master of Science,” 2020.

[99] R. Mendelsohn, “Fourier Transform Infrared Spectrometry, 2nd ed By Peter R. Griffiths (University of Idaho, Moscow) and James A. De Haseth (University of Georgia, Athens). J. Wiley & Sons, Inc.: Hoboken, NJ. 2007. xviii + 530 pp. $ 115. ISBN 978-0-471-19404-0.,” *J. Am. Chem. Soc.*, vol. 129, no. 43, pp. 13358–13358, Oct. 2007, doi: 10.1021/ja076968d.

[100] S. E. Colthup, N. B.; Daly, L. H.; Wiberley, *Introduction to Infrared and Raman Spectroscopy*, 3rd Editio. 1990.

[101] L. Ohlin, *An in-situ ATR-FTIR Spectroscopy Study of Adsorption in MFI Zeolites*. 2015.

[102] F. M. Mirabella, *nternal reflection spectroscopy: theory and applications.* 1993.

[103] G. Binnig, C. F. Quate, and C. Gerber, “Atomic Force Microscope,” *Phys. Rev. Lett.*, vol. 56, no. 9, pp. 930–933, Mar. 1986, doi: 10.1103/PhysRevLett.56.930.

[104] N. Jalili and K. Laxminarayana, “A review of atomic force microscopy imaging systems: application to molecular metrology and biological sciences,” *Mechatronics*, vol. 14, no. 8, pp. 907–945, Oct. 2004, doi: 10.1016/j.mechatronics.2004.04.005.

[105] A. Aliano *et al.*, “AFM, Tapping Mode,” in *Encyclopedia of Nanotechnology*, Dordrecht: Springer Netherlands, 2012, pp. 99–99.

[106] R. García, “Dynamic atomic force microscopy methods,” *Surf. Sci. Rep.*, vol. 47, no. 6–8, pp. 197–301, Sep. 2002, doi: 10.1016/S0167-5729(02)00077-8.

[107] L. Potential, “Mod Contact mode e No tes.”

[108] C. J. Wright, L. C. Powell, D. J. Johnson, and N. Hilal, “MICROSCOPY | Atomic Force Microscopy,” in *Encyclopedia of Food Microbiology*, Elsevier, 2014, pp. 666–675.

[109] P. Pattojoshi, G. S. Roy, A. Editor, and S. Joseph, “Handbook of Nanotechnology of Nanotechnology,” pp. 1–17, 2020.

[110] B. Bhushan, Ed., *Nanotribology and Nanomechanics I*. Berlin, Heidelberg: Springer Berlin Heidelberg, 2011.

[111] Lord Kelvin, “V. Contact electricity of metals,” *London, Edinburgh, Dublin Philos. Mag. J. Sci.*, vol. 46, no. 278, pp. 82–120, Jul. 1898, doi: 10.1080/14786449808621172.

[112] B. Bhushan and M. L. B. Palacio, “Kelvin Probe Force Microscopy,” in *Encyclopedia of Nanotechnology*, Dordrecht: Springer Netherlands, 2012, pp. 1173–1179.

[113] W. Melitz, J. Shen, A. C. Kummel, and S. Lee, “Kelvin probe force microscopy and its application,” *Surf. Sci. Rep.*, vol. 66, no. 1, pp. 1–27, 2011, doi: 10.1016/j.surfrep.2010.10.001.

[114] R. Shikler, T. Meoded, N. Fried, B. Mishori, and Y. Rosenwaks, “Two-dimensional surface band structure of operating light emitting devices,” *J. Appl. Phys.*, vol. 86, no. 1, pp. 107–113, Jul. 1999, doi: 10.1063/1.370706.

[115] A. Ulman, *An Introduction to Ultrathin Organic Films*. Elsevier, 1991.

[116] M. D. Porter, T. B. Bright, D. L. Allara, and C. E. D. Chidsey, “Spontaneously organized molecular assemblies. 4. Structural characterization of n-alkyl thiol monolayers on gold by optical ellipsometry, infrared spectroscopy, and electrochemistry,” *J. Am. Chem. Soc.*, vol. 109, no. 12, pp. 3559–3568, Jun. 1987, doi: 10.1021/ja00246a011.

[117] E. Luboch, J. F. Biernat, Y. A. Simonov, and A. A. Dvorkin, “Synthesis and electrode properties of 16-membered azo- and azoxycrown ethers. Structure of tribenzo-16-azocrown-6,” *Tetrahedron*, vol. 54, no. 19, pp. 4977–4990, May 1998, doi: 10.1016/S0040-4020(98)00203-8.

[118] D. R. Armstrong, J. Clarkson, and W. E. Smith, “Vibrational analysis of trans-azobenzene,” *J. Phys. Chem.*, vol. 99, no. 51, pp. 17825–17831, 1995, doi: 10.1021/j100051a005.

[119] K. Okuno, T. Ito, M. Iwami, and A. Hiraki, “Presence of critical Au-Film thickness for room temperature interfacial reaction between Au(film) and Si(crystal substrate),” *Solid State Commun.*, vol. 34, no. 6, pp. 493–497, 1980, doi: 10.1016/0038-1098(80)90659-6.

[120] J. F. Chang, T. F. Young, Y. L. Yang, H. Y. Ueng, and T. C. Chang, “Silicide formation of Au thin films on (1 0 0) Si during annealing,” *Mater. Chem. Phys.*, vol. 83, no. 2–3, pp. 199–203, 2004, doi: 10.1016/S0254-0584(03)00240-2.

[121] A. Hiraki, K. Shuto, S. Kim, W. Kammura, and M. Iwami, “Room-temperature interfacial reaction in Au-semiconductor systems,” *Appl. Phys. Lett.*, vol. 31, no. 9, pp. 611–612, Nov. 1977, doi: 10.1063/1.89799.

[122] D. Nowak *et al.*, “Nanoscale chemical imaging by photoinduced force microscopy,” *Sci. Adv.*, vol. 2, no. 3, p. e1501571, Mar. 2016, doi: 10.1126/sciadv.1501571.

[123] V. A. Tamma, F. Huang, D. Nowak, and H. Kumar Wickramasinghe, “Stimulated Raman spectroscopy and nanoscopy of molecules using near field photon induced forces without resonant electronic enhancement gain,” *Appl. Phys. Lett.*, vol. 108, no. 23, p. 233107, Jun. 2016, doi: 10.1063/1.4952738.